CRSS-03/06
June 30, 2003

Limits of Coolability in the AP1000-Related ULPU-2400 Configuration V Facility

T-N. Dinh, J.P. Tu, T. Salmassi, T.G. Theofanous

Center for Risk Studies and Safety
University of California, Santa Barbara
6740 Cortona Drive, Goleta CA 93117

Work performed under grant from U.S. Department of Energy
International Nuclear Energy Research Initiative
K-NERI program

UCSB

CRSS-03/06
June 30, 2003

Limits of Coolability in the AP1000-Related ULPU-2400 Configuration V Facility

T-N. Dinh, J.P. Tu, T. Salmassi, T.G. Theofanous

Center for Risk Studies and Safety
University of California, Santa Barbara
6740 Cortona Drive, Goleta CA 93117

Work performed under grant from U.S. Department of Energy
International Nuclear Energy Research Initiative
K-NERI program

UCSB

Executive Summary:

This report documents experimental results obtained at the University of California, Santa Barbara (UCSB) on ULPU facility Configuration V. The work was supported by Westinghouse and by the U.S. Department of Energy's International Nuclear Energy Research Initiative (I-NERI) program. It was performed within the scope of a K-NERI project on "In-Vessel Retention" (IVR).

Briefly, IVR is a scheme for severe accident management in which the reactor pressure vessel lower head is submerged in water-flooded reactor cavity, and the so-obtained external vessel cooling is used to arrest the vessel melt attack. Central to the whole concept is the limit of coolability determined by critical heat flux (CHF) on the external vessel surface. Such CHF data were first measured in ULPU – a unique, full-scale facility that was originally built to simulate AP600 geometry and cavity flooding conditions (Theofanous et al, 1996). More recently, 28 experiments were performed on ULPU Configuration IV facility in which the flow path around the lower head was streamlined. The ULPU-IV experimental results were documented, distributed (Theofanous et al, 2002a) and used as support of the IVR case for AP1000 certification. These data show that flow path streamlining is beneficial for IVR performance as indeed needed for higher (than AP600) power reactors such as AP1000.

On this basis, Westinghouse adopted the concept of a thermal insulation design that would create such a streamlined flow path, and the present work was to consider optimization of this path within the specific geometric features of the AP1000 reactor cavity design (especially concerning the exit geometry). To ensure that the CHF is reached, even at the so-enhanced performance, peak flux capability was upgraded from ~2 MW/m^2 to ~2.4 MW/m^2. Thus ULPU-2400 Configuration V (abbreviated as ULPU-V) came into being.

Tipped from recent work in our BETA experiment (Theofanous et al, 2002b-2002c), we anticipated important effects of heater surface nanomorphology, which called for special attention to achieving good control of the chemical composition of the coolant. Thus we replaced parts as needed, so as to have a thoroughly cleansed (and cleanable) all glass and stainless steel structure. This structure was fitted by the copper block heaters, again with special attention paid to the selection of gasket material, so as to ensure absence of contamination.

A total of thirty-six experiments in three test series have been carried out so far, and are reported in detail here. Besides the temperature/power histories, and CHF determination for each run, we report natural circulation flow rates, pressures and pressure differentials around the loop, and provide spectral information on these time-series data. The three series of tests addressed flow path dimensions around the lower head (baffle positioning), power shape, and water chemistry respectively. Auxiliary data on water chemistry were obtained in the basics-oriented (upwards-facing flat plate geometry) BETA experiment. The CHF data and understanding derived thereof robustly enhance the coolability limits found in the AP600 geometry, and add additional margins to those found in Configuration IV (especially eliminating the there-found "exit phenomenon").

Moreover, the present results indicate that the currently foreseen exit geometry in AP1000 is restrictive, in that the natural-circulation-obtained flow rate is saturated with input power over essentially the whole relevant operational domain. It is in our near-future plan to determine the extent of additional margins that elimination of this exit restriction would entail.

A basic advance that was made in this work concerns the effects of heater surface nanomorphology and coolant chemistry. We found that a totally clean (de-ionized) coolant is able to promote such a degree of "cleansing" of the heater surface as to have a rather significant deleterious effect on the CHF. At the other extreme, the presence of TSP (tri-sodium-phosphate), a typical dissolved substance in reactor cavity water (an alkaline solution) has an outstanding beneficial effect on CHF. The presence of Boric Acid, also a normal ingredient here, diminished somewhat this enhancement, but still the CHF is considerably higher than that with pure water. While not observed previously, these trends are consistent with the basic origin of burnout, as is developing from our understanding in our co-current NASA-funded work carried out in BETA with nanofilm heaters, under controls much stricter than is possible with a large-scale facility such as ULPU (Theofanous et al, 2002 b-c).

Finally, from the pressure data, analytical interpretations thereof, and visual observations, we developed information on dynamic loads, as needed for the structural design of the thermal insulation. We conclude that the main energy content of the pressure fluctuations is found in two frequencies. One is at 0.2 Hz and underlies a flow regime instability that is due to the flow path restriction (and geometry) at the exit. The result is a periodic change in the upper ~2 meters of the flow path, from low quality liquid flows to a flashing front that initiates at the exit and moves downward, establishing a highly-voided two-phase flow, until it is swept out at the beginning of a new cycle. The other dominant frequency is at around 1 Hz. It occurs in the heated section (around the vessel lower head) and it is due to the highly non-equilibrium subcooled boiling (simultaneous evaporation and condensation). In this region the resulting pressure fluctuation is highest, about ±0.5 m of water column. Further information on loads can be found in the complete spectra of pressure fluctuations presented over the wide range of power input conditions covered by these ULPU-2400 runs.

Table of Contents

ACRONYMS

ACOPO	a IVR-related 1/2 -scale natural convection facility at UCSB
BETA	pool boiling burnout experiments at UCSB
BA	Boric Acid
CHF	Critical Heat Flux
CRSS	Center for Risk Studies and Safety at UCSB
DI	de-ionized water
FFT	Fast Fourier Transform
IVR	In-Vessel Retention
TSP	Tri-Sodium-Phosphate
UCSB	University of California at Santa Barbara
ULPU	a IVR-related full-scale boiling heat transfer facility at UCSB
ULPU-V	ULPU-2400 Configuration V facility

NOMENCLATURE

CHF	critical heat flux, kW/m^2 or MW/m^2
G	flow rate, m^3/min
P	pressure, m of water column
q	heat flux, kW/m^2
Q	total input power, kW
T	temperature, °C
x	equilibrium quality, -
θ	angular position on the lower head from the lower pole, degree (°)

ACKNOWLEDGEMENT

The work described in this report was supported by Westinghouse Electric Company and the U.S. Department of Energy's International Nuclear Energy Research Initiative Program (I-NERI) under contract DE-FG06-02RL14337. The BETA facility was developed for NASA under grants NAG3-2119 and NAG3-2761.

1. INTRODUCTION

The present work is part of a research program at the University of California-Santa Barbara (UCSB), aiming to develop a basic understanding and create a foundation to allow implementation of the In-Vessel Retention (IVR) concept to high-power reactors. The IVR technology was first introduced at UCSB during 1989-1996 as a Severe Accident Management Strategy in the Lovissa reactors currently operating in Finland, and in Westinghouse's Advanced LWR design of AP600 (Theofanous et al, 1996), which was recently certified by the US Nuclear Regulatory Commission. Briefly, the IVR process involves flooding the reactor cavity (in a core meltdown sequence) to retain the molten core within the reactor pressure vessel (RPV) boundary. One of key elements of the IVR technology is the limit of coolability expressed by critical heat fluxes (CHF) on the external vessel surface. For the AP600, such limits to coolability were determined in experiments performed on a full-scale simulation facility named ULPU-2000 at UCSB (Theofanous et al, 1997).

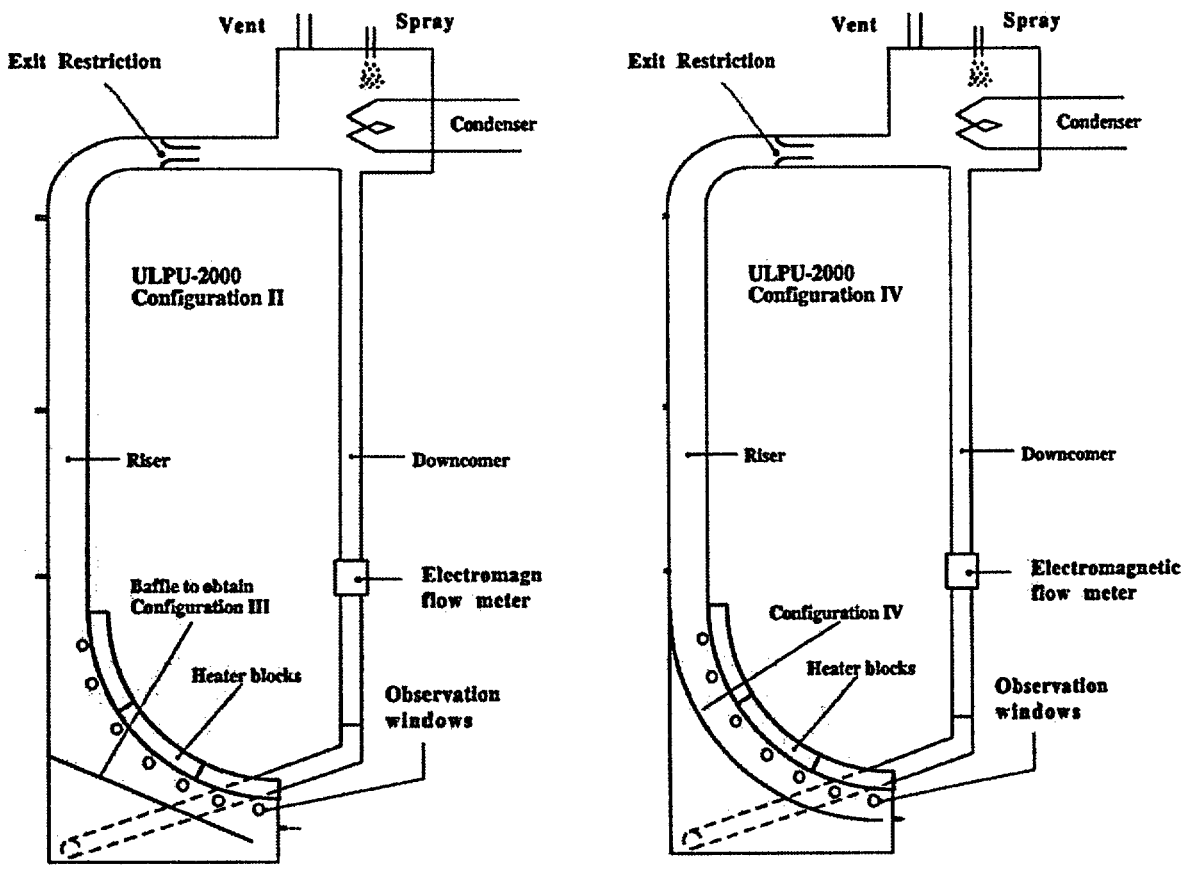

Figure 1.1. Schematics of the ULPU-2000 Configurations III and IV.

Previous work conducted on ULPU-2000 facility Configuration I, II and III, created a basic understanding of burnout on downward facing heaters and provided support for the

assessment of IVR for AP600 design (Figure 1.1). Extensive visual observations of two-phase flow in ULPU experiments indicated potential for enhancement of limit of coolability. Such enhancement is needed if the IVR technology is to be applied to higher power (compared to AP600) reactors. In search for improving the IVR technology, we looked into the effect of the flow path that allows water to circulate around the lower head and up towards the top of the reactor vessel. During the year 2002, we incorporated into the ULPU-2000 facility a baffle simulating an alternate (than usual) geometry of the reflecting insulation around the RPV. The baffle serves to streamline the flow path between the RPV surface and the insulation. The resulting Configuration is named ULPU-IV and also shown in Figure 1.1 for comparison.

In total, twenty eight (28) burnout experiments were conducted on ULPU-IV facility. ULPU-IV results show that streamlining the flow path around the lower head enhances convection and is beneficial to CHF performance under IVR conditions. Description of ULPU-IV facility and ULPU-IV experimental results were documented in a technical report by Theofanous et al (2002), distributed, and used in Westinghouse's assessment of IVR for AP1000 design certification. It is noted, however, that flow channel geometry in ULPU-IV facility was not specifically designed to match AP1000 geometry and flow conditions. Figure 1.2 depicts an IVR schematic for AP1000. It can be seen that the geometry of flow entry into the baffle region and exit from the riser are not simulated in ULPU-IV. In fact, during the year 2002, design of thermal insulation and related components in AP1000 continued to evolve. Notably, geometry of four flow channels which exit from annular space between thermal insulation and reactor vessel have changed from L-shape duct (circle A) into 22°-inclined duct (shown in insert B of Figure 1.2). It is expected that complex geometries of flow inlet and exit from thermal insulation may affect two-phase natural circulation flow in IVR, and ultimately, to the CHF performance.

The present investigation follows Westinghouse's adoption of the streamlined flow path concept for IVR in AP1000, and is a continuation of the previous work. Aiming to accurately represent the effect of AP1000 geometry on limits of coolability under IVR, the authors collaborated with Westinghouse engineers in developing a way to simulate the AP1000 IVR geometry in ULPU-V facility. Detailed description of the facility modifications compared to ULPU-IV facility is given below (section 2). The power system in ULPU-2000 was also upgraded to allow reliable operation at higher maximum heat fluxes (up to ~2400 kW/m^2) expected in ULPU-V facility. Further, these modifications, including the positioning of the curved baffle around the lower head were made flexible to allow for design changes and optimization. Thirty six burnout experiments were conducted on the new ULPU-2400 Configuration V facility (abbreviated as ULPU-V), using three baffle positions. Critical heat fluxes exceeding 1.8 MW/m^2 were obtained.

In what follows, we describe the ULPU-V facility, emphasizing major features that simulate AP1000 IVR geometry (section 2). We then go on to present the experimental program and main results obtained (section 3). The detailed experimental data for each of the ULPU-V test runs are given in Appendix C. Section 4 describes a program of supporting (BETA) experiments and their results. Synthesis of ULPU-V and BETA test results is given in section 5, followed by a listing of our conclusions and recommendations (section 6).

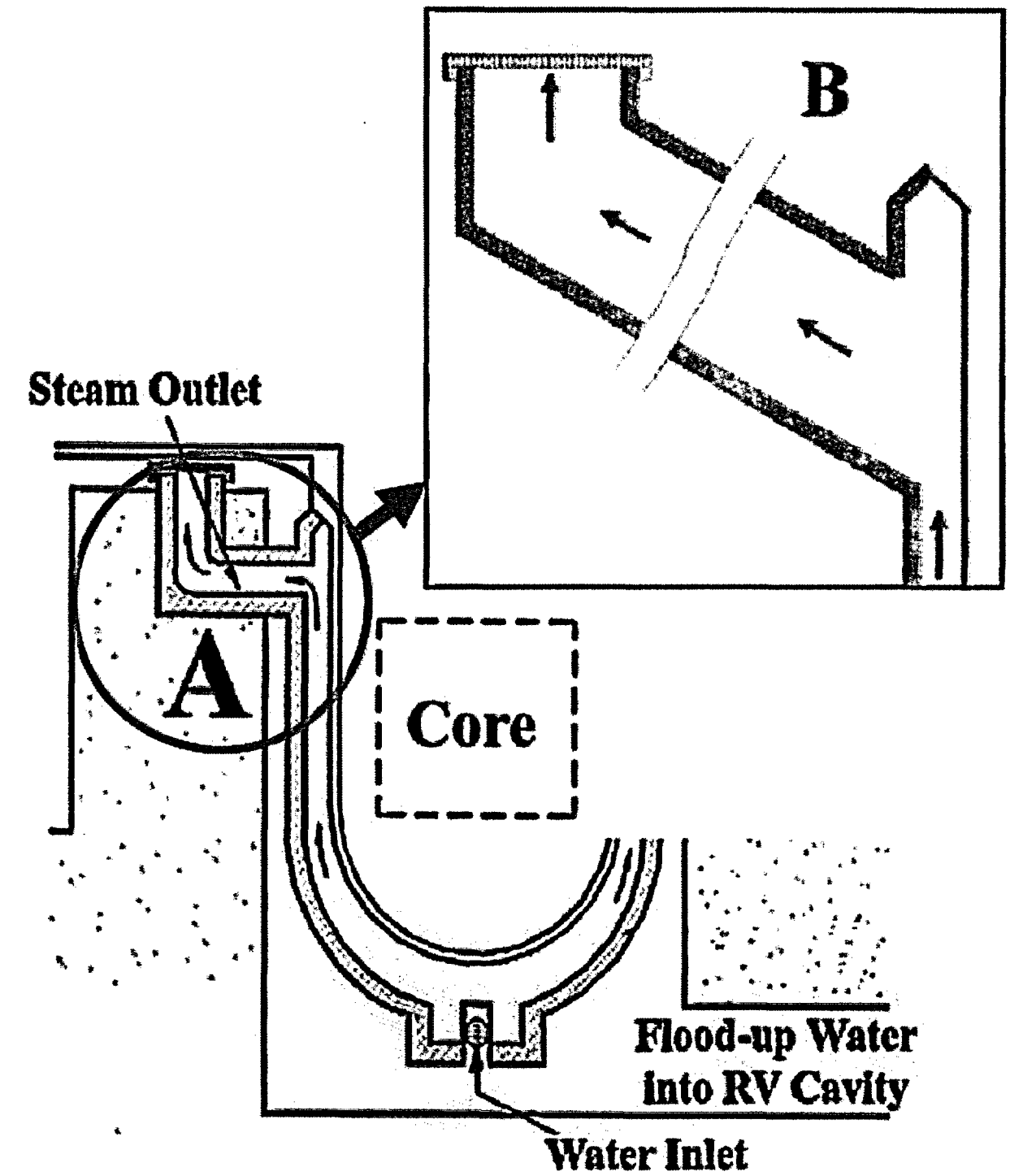

Figure 1.2. Representation of AP1000 design geometry (courtesy of J. Scobel)

2. TEST FACILITY AND EXPERIMENTAL APPROACH

The ULPU-V experimental concept is similar to that used in ULPU-III and ULPU-IV programs. It is based on the idea that boiling/condensation phenomena that define the coolability limits under IVR, are affected by local flow and subcooling conditions, so representing the full length of the flow path (gravity head) is quite essential for proper simulation. We use a similarity rule that matches the local quality (that is, the integral of upstream power) to map any reactor power shape to an ULPU power shape for testing the critical heat flux—this mapping changes with the angular position being tested. Detailed description of the power shaping principle in ULPU was given in Theofanous and Syri (1997) and in Theofanous et al (2002a).

The ULPU approach allows us to achieve an effective full-scale simulation of the reactor axisymmetric geometry, by the ULPU slice geometry. The reactor vessel is simulated by custom-made, 76 mm thick, 152 mm wide copper blocks and power input is provided by embedded cartridge heaters that are individually controlled to create any heat flux shape at will. It is noted that due to the copper block's large thermal inertia (76 mm thick), it is very easy to recover from the temperature excursion that marks the boiling crisis, and be ready for another run within minutes. This allows for a very fine resolution of the coolability limits and thorough testing of experimental parameters. At the uppermost end of the copper heated block, the 15-cm wide heater represents 1:84 portion of the AP1000 vessel perimeter. This ratio of 1:84 is used for geometrical scaling of flow channel in the slice facility ULPU-V relative to prototypic AP1000 design.

The ULPU-V facility is shown in Figures 2.1-2.2, and schematic only in Figure 2.3. It is a full-length representation of a reactor lower head and the whole flow path between the reactor vessel and reflecting thermal insulation, all the way to the top venting openings. In prototypic reactor geometry, the "downcomer" consists of large size cavities and connecting ducts with virtually no flow resistances. In ULPU-V the downcomer is represented by a 6" pipe (152 mm in diameter), which replaced the 3" pipe used in ULPU-IV. All but one elbow in the downcomer are eliminated to further reduce local pressure losses. In the downcomer's uppermost section, a second branch is added to reduce entry flow velocity, and eliminate the vorticity induced gas entrainment into the downward flow (see Figure 2.3). The electromagnetic flowmeter mounted on the downcomer (Figure 2.3) is Venturi type with 4" throat that insures insignificant pressure losses. Subsequent flow visualization confirms that a gas entrainment into downcomer observed in some of the ULPU-IV tests is fully eliminated. Also, pressure measurements confirm minimal friction losses in downcomer.

The uprising branch in IVR coolant natural circulation loop in AP1000 includes three major sections: curved channel around the vessel lower head, annular channel along the RPV cylindrical part, and inclined channel which connects the thermal insulation to the containment's upper coolant pool (see Figure 1.2). In ULPU-IV and V facility a "riser" is used to simulate the full length of the reactor vessel to the top flange (~6 m). The riser is made with 152 mm in diameter Pyrex glass that allows visualization. The glass is industrial strength, rated at 60 psig, so that operating at some moderately increased pressure level is

feasible. The riser diameter was selected to effectively match the hydraulic diameter of annular flow area between thermal insulation and reactor pressure vessel.

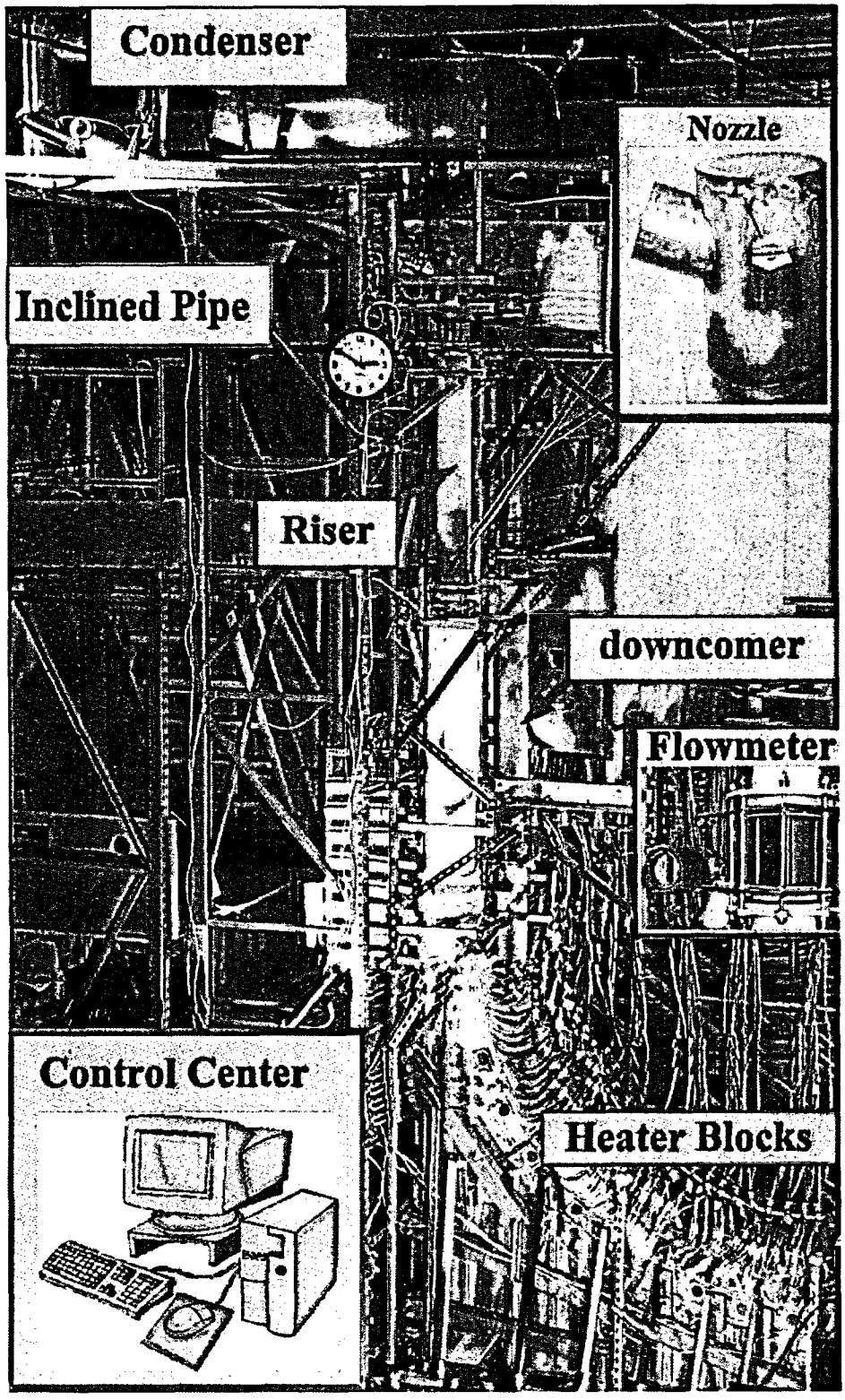

Figure 2.1. Overview of the ULPU-2400 facility.

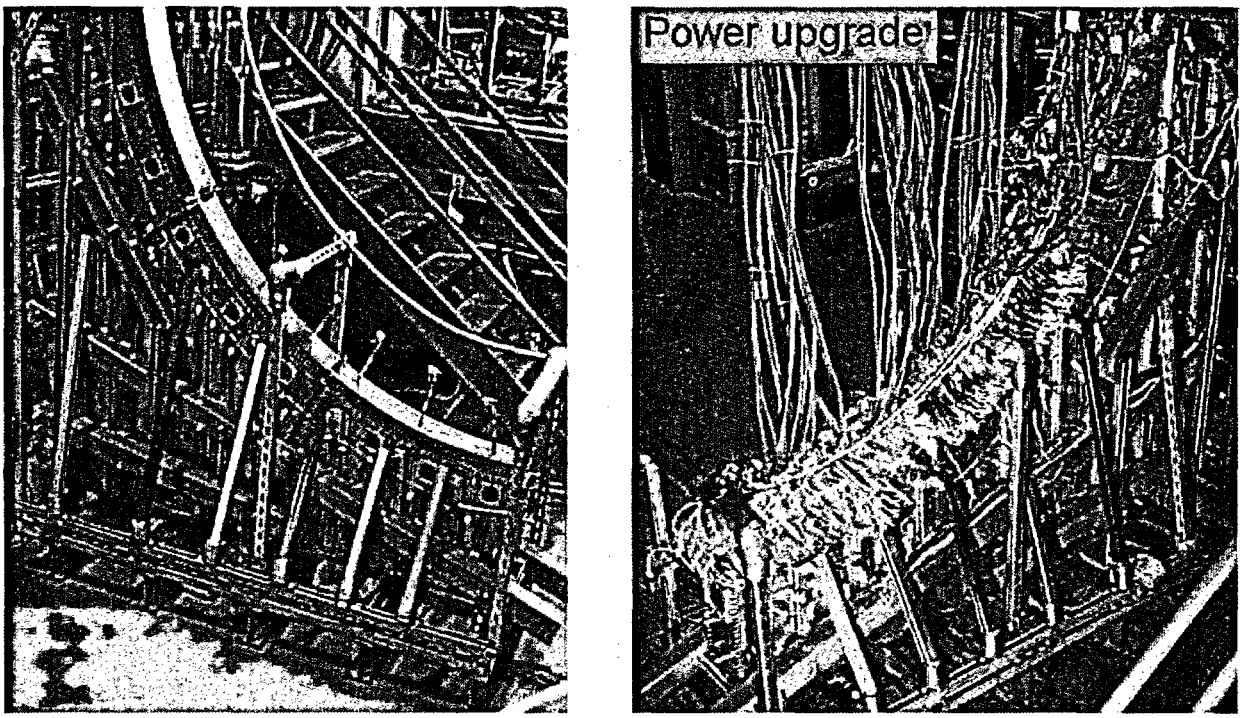

Figure 2.2. ULPU-2400 facility – upgraded power and heating systems. The copper blocks and cartridge heaters were custom-made and upgraded to allow a maximum total power of 500 kW and local heat flux of up to ~2400 kW/m^2. The name ULPU-2400 is to reflect this capability in Configuration V.

To achieve an accurate representation of IVR-related flow geometry in AP1000 significant modifications were made in the uprising branch in ULPU facility; these modifications were developed in collaboration with Westinghouse's AP1000 engineers. Remarkably, discussion of the design modification in ULPU actually led to evolution in AP1000 plant design. An example is shown in Figure 1.2 for the steam outlet configuration. Compared to ULPU-IV, four major modifications made in the ULPU uprising branch are

(i) inlet baffle and baffle entry,
(ii) adjustable baffle around the vessel lower head,
(iii) smooth transition from baffle to riser, and
(iv) nozzle that simulates transition from the riser to inclined duct.

Detail description of design and operation of these components are discussed below.

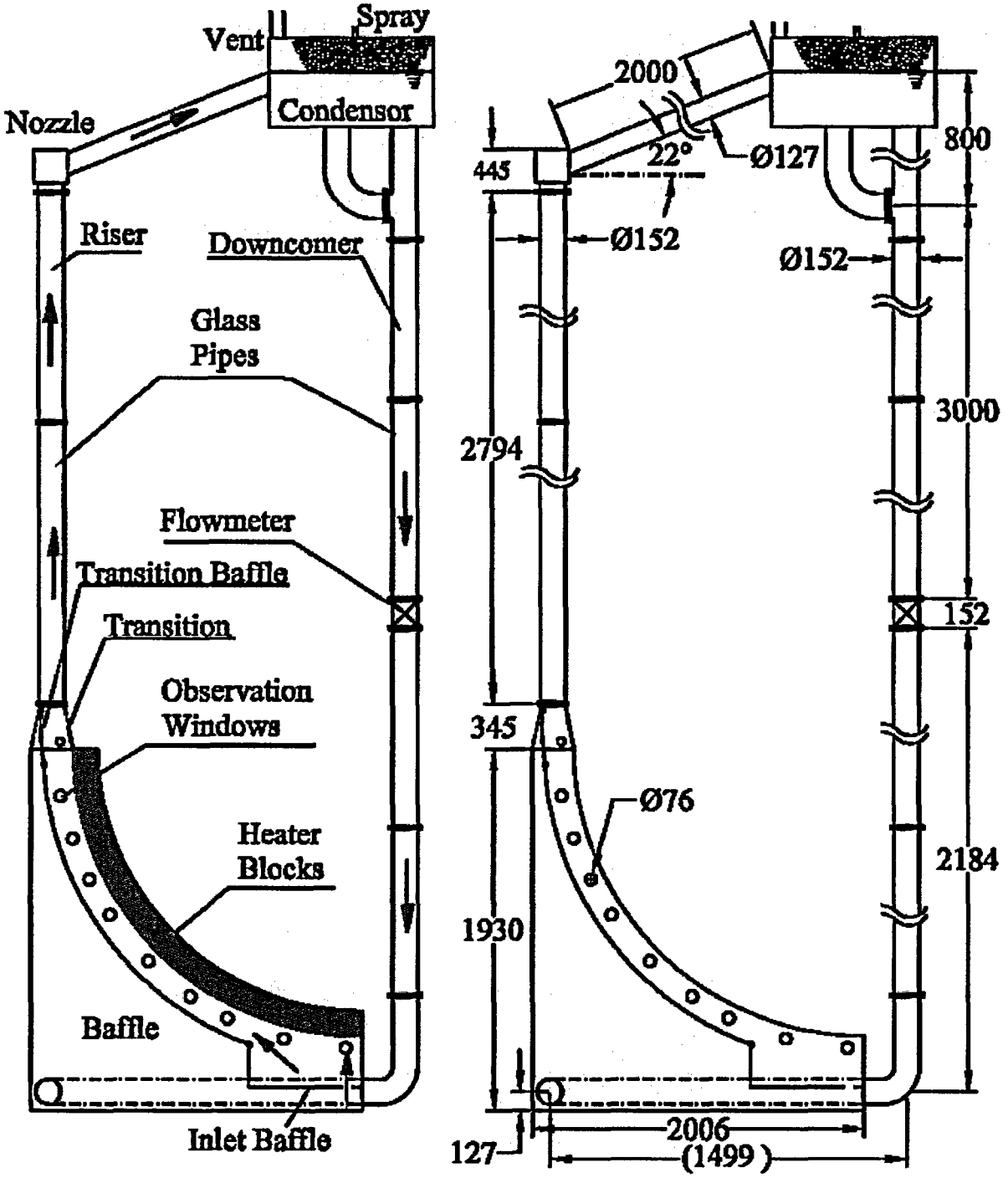

Figure 2.3. Schematics of the ULPU-2400 facility – Configuration V. For clarity we show separately the system components (left) with arrows depicting flow direction, and dimensions (right). All dimensions in mm, not to scale. Note that in 3D the horizontal pipe (1499) from the downcomer to bottom cavity is at the right angle to the paper plane.

Inlet baffle and baffle entry

In ULPU-V an inlet baffle was introduced to represent a similar structure beneath the lowermost region of the reactor vessel lower head. In prototypic AP1000 design, the inlet baffle is a part of thermal insulation and must be closed during the plant's normal operation (see Figure 1.2). However, the IVR operation requires an open flow area for coolant to enter and circulate in the flow channel between the curved baffle and the vessel surface. Westinghouse engineers have developed a concept of floating balls to achieve the dual objectives of holes in the inlet baffle. In ULPU-V the baffle entry is represented by a 3" hole (76 mm in diameter) that gives ≅1:84 of flow areas provided by openings in the inlet baffle in AP1000 IVR design. While the inlet baffle is fixed, its connection to the curved baffle is flexible, to allow the adjustment of the curved baffle position.

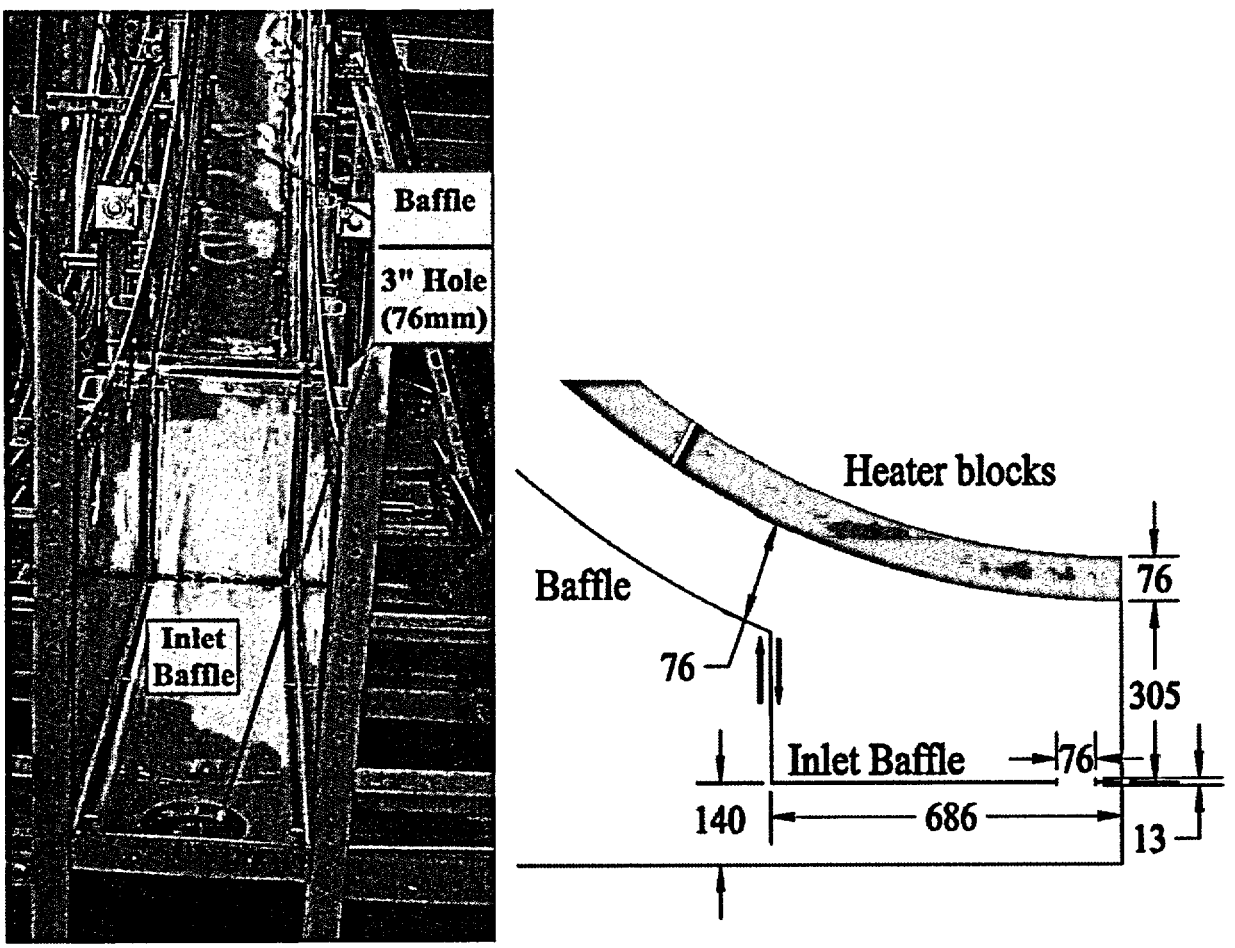

Figure 2.4. AP1000 inlet baffle representation in ULPU-2400 Configuration V. The arrows show a vertical segment of the curved baffle slide (adjustable) on the vertical segment of the inlet baffle (fixed).

Adjustable baffle around the vessel lower head

A curved baffle for coolant flow streamlining was first designed and tested in ULPU-IV facility. In the present work, the baffle was designed with a positioning mechanics that allows flexible changes of the baffle-vessel surface distance. Such an approach to the baffle design in ULPU-V was necessary for optimization. In the ULPU-V program three baffle configurations are employed as shown in Figure 2.5: two configurations (named 3" and 6") have equi-distant flow channels with 3" (76 mm) and 6" (152 mm) depth, and the third configuration has 3" distance in the lowermost point of the curved baffle and 6" distance to the uppermost point of the heater section.

In addition, a leak-tight contact between baffle edges and the "cavity" sidewalls was achieved in ULPU-V to eliminate any leakage flow between cavity and flow channel – the two chambers on two sides of the baffle. The key here is to ensure accurate measurement of local pressure in two-phase flow and prevent side effects due to spurious inflow of subcooled water from the "reactor cavity" chamber.

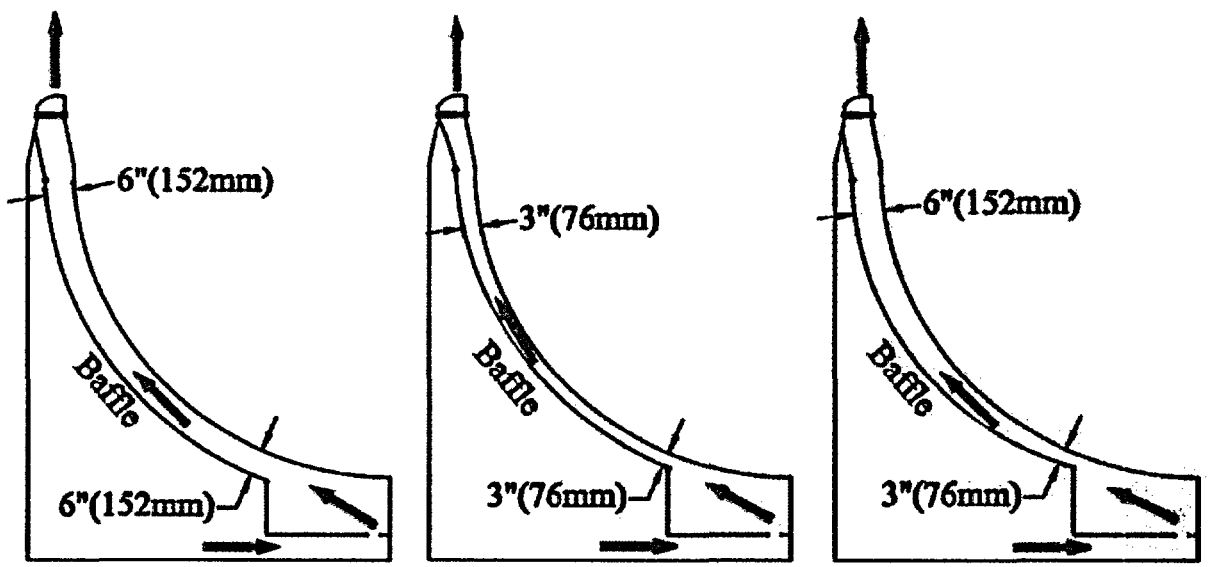

Figure 2.5. AP1000 thermal insulation representation in ULPU-2400 Configuration V. Three baffle positions, with baffle-to-heater distances being 6", 3", and 6"-to-3".

Transition from the curved baffle to riser

It is noted that ULPU-IV experiments showed an enhancement over the whole region of vessel lower head but in the uppermost section. This behavior, named "exit phenomenon" in Theofanous et al (2002a), was analyzed in order to investigate mechanisms responsible for it. It was noted that the 9" distance from the baffle to heater in the uppermost region and its transition to 6" pipe of the riser in ULPU-IV may have been responsible for this singular

behavior. Specifically, the flow area changed from 345 cm^2 to 181 cm^2. Perhaps more importantly, the flow momentum is reduced due to vapor condensation that takes place beyond the heater end.

As it can be seen from Figure 2.5, the flexible baffle design in ULPU-V facility allows a smooth transition from the curved baffle into the riser's pipe. Notably, in the ULPU-V program baffle-to-heater distances of 3" and 6" at the uppermost location were employed. As it will be shown in the ULPU-V experimental results (section 3 below), the "exit" phenomena were significantly reduced in sub-series M3 and M6 and practically eliminated in sub-series M63. This result presents a major enhancement in ULPU-V CHF over ULPU-IV CHF.

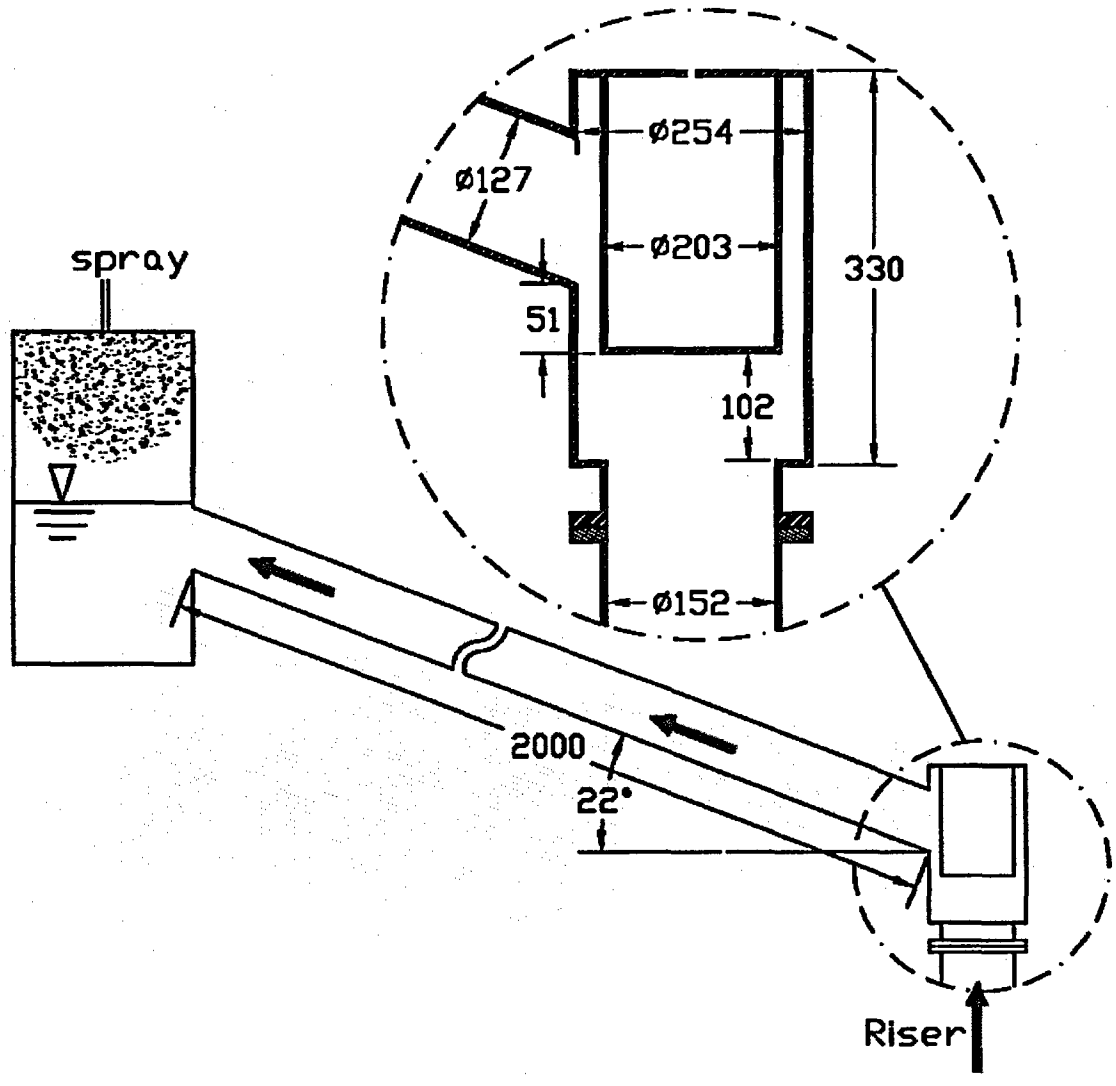

Figure 2.6. AP1000 exit from riser represented in ULPU-2400 Configuration V.

Nozzle (transition from riser to inclined duct)

In AP1000 prototypic reactor geometry, coolant outlet from the annular riser is provided by four large-size rectangular ducts emanating from the thermal insulation (Figure 1.2). Such a flow organization requires the flow to change direction from uprising to convergent into the four outlets. Notably, within the riser the coolant flow is dominantly single phase flow due to significant water-column-induced subcooling that is present in the system. However, local pressure in the riser's upper section is reduced enough to initiate flashing and create two-phase flow when levels of input power are sufficiently high. In the ULPU slice geometry, the transition from the annular riser to the inclined duct is represented by an annular nozzle as shown in Figure 2.6. The purpose of having an internal cylinder before the flow entry into the inclined pipe is to represent the momentum effect of upward flow momentary stagnation and re-direction in the prototypic reactor geometry. The annular space between the internal cylinder and external shell is designed to match the effective hydraulic diameter (152 mm) of flow channel in the annular space of thermal insulation. The diameter of the 5" inclined pipe (127 mm) is chosen on the geometrical scaling basis that is 1:84 to the total flow area provided by four ($0.5x0.5m^2$) ducts.

Power shaping and burnout testing procedure

To adequately represent two-phase flow conditions at a particular angular position in slice ULPU geometry versus that of hemispherical geometry of the reactor lower head, the same power shaping principle developed for AP600 is applied in ULPU-III, ULPU-IV and now ULPU-V. We use a reference thermal load from the ACOPO experiments (also at UCSB), and a power profile that allows the flow enthalpy at the tested angular position be matched (Figures 2.8-2.9). The power profile is also given for each test in Appendix C.

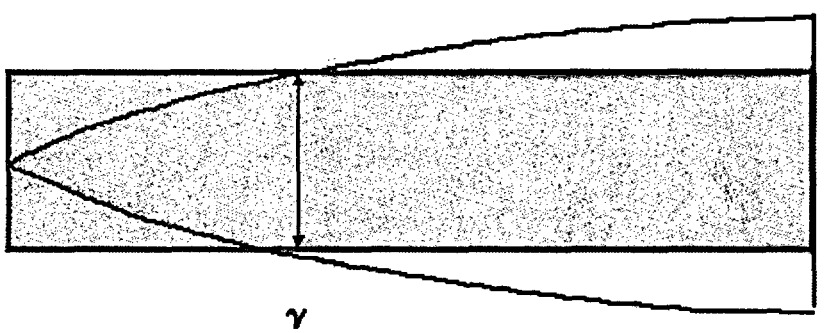

Figure 2.8. Heat flux shaping principle.

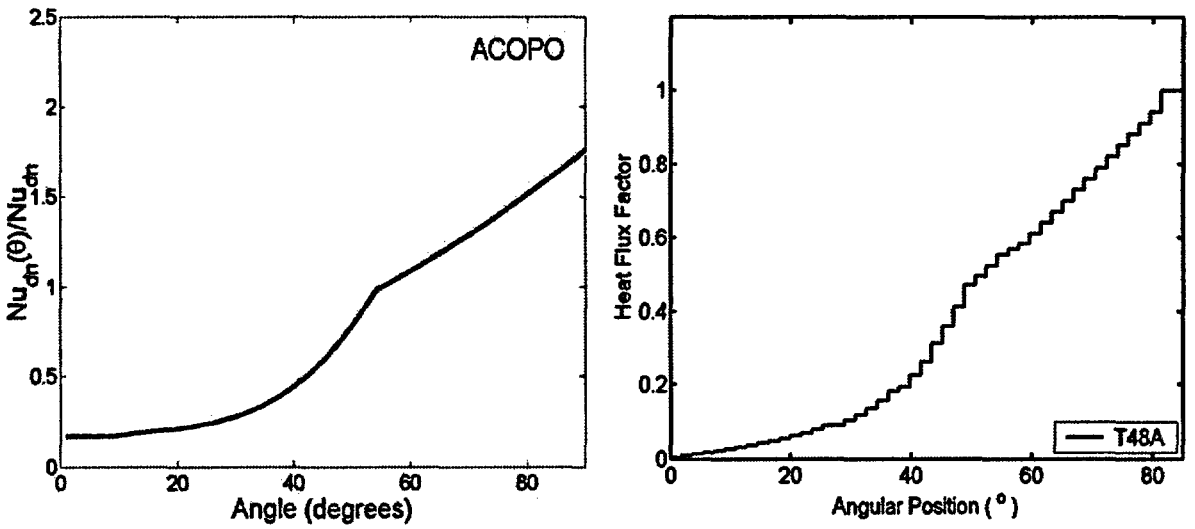

Figure 2.9. Reference thermal load based on ACOPO data (left) and example of corresponding heat flux shaping for 80-85°.

It should be noted that in the ULPU-V test program, several new power profiles were added, as compared to power profiles used in ULPU-III and ULPU-IV. Specifically, T40D, T40E, and T40F are modified from T40B (Figure .2.10) The latter power profile was designed to quantify CHF at 66-71° region of the vessel lower head. The new profiles were designed with higher heat fluxes in the upstream region to allow the effect of power shaping to be tested. Similarly, we have T48B and T48C profiles as modification of T48A designed for CHF testing at 80-84° (see Figure 2.11).

The data in Appendix C show the power stepping employed in each step, and from these one can deduce the uncertainty in quoted CHF values. In particular, for the most relevant M63 test series, the CHF was bracketed within 3%, 5%, and 7% for run #8, #9, and #10 respectively. By comparison, the measurement error of ~1% is negligible. Heater resistance is measured before and after each run to ensure that no heater loss remains undetected.

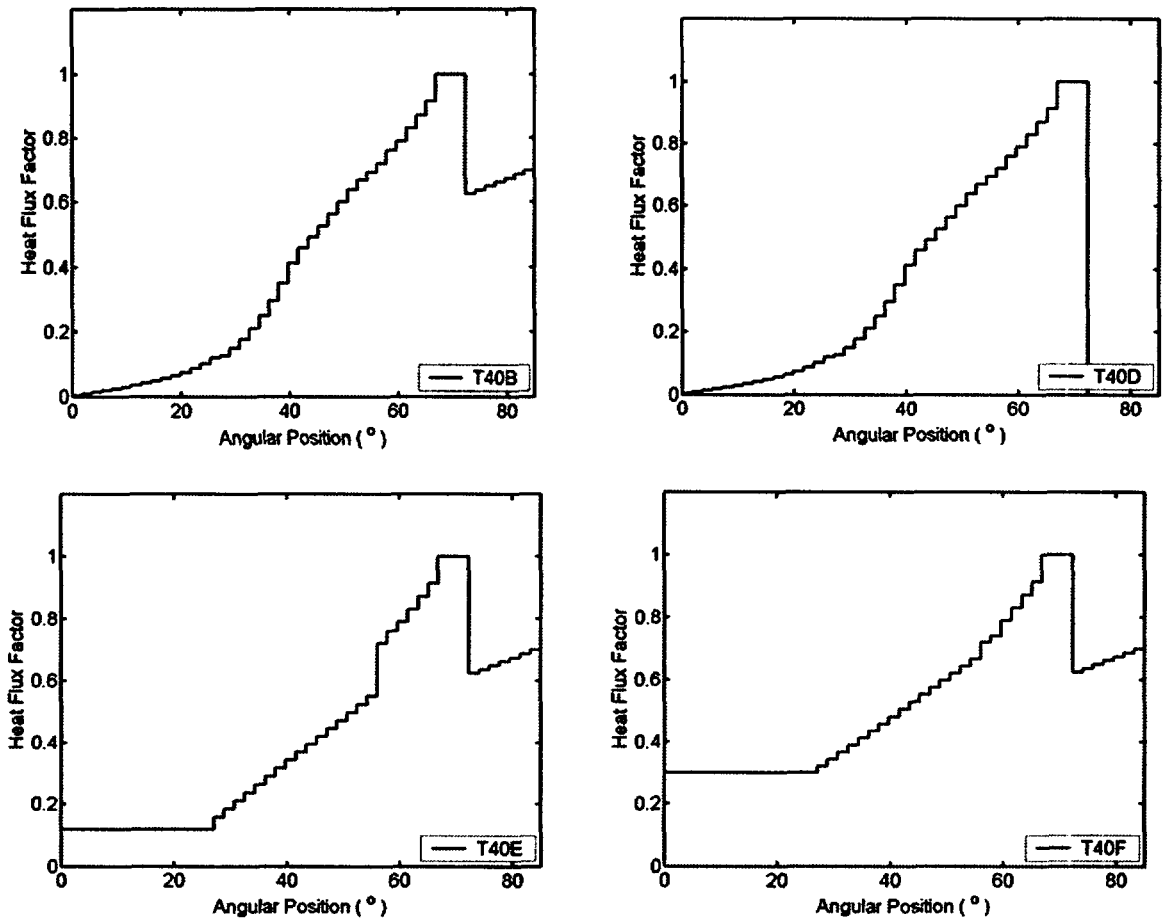

Figure 2.10. Original power shape T40B and modified power shapes: T40D (cut-off downstream), T40E (20% enhanced upstream), and T40F (40% enhanced upstream).

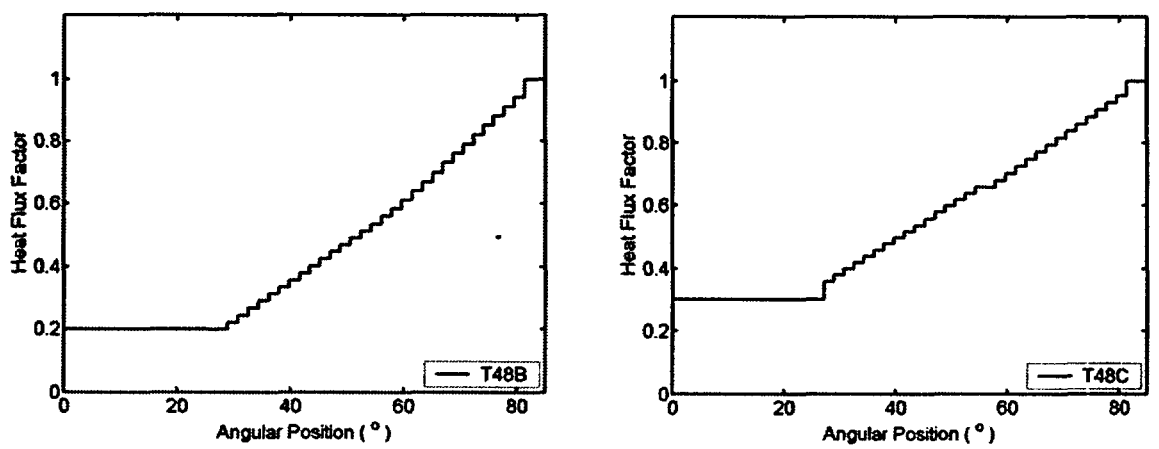

Figure 2.11. Modified power shapes: T48B (20% enhanced upstream), and T48CF (40% enhanced upstream) for the original power shape T48A (shown in Figure 2.9).

Instrumentation and measurement.

.The basic instrumentation in ULPU-V is straightforward, and includes thermocouples, pressure transducers, and an electromagnetic flow meter. In addition, the transparent downcomer and riser, and observation windows on the walls of the curved baffle region allow direct visualization and high speed video recording of the flow regimes.

Thermocouples employed are Omega K-type. Positioning within the heater blocks is depicted in Appendix A. Positioning within the coolant at several locations around the flow loop is indicated in Figure 2.12. In all these thermocouples the tip is placed midway in the flow channel. Data acquisition was set at 0.25 Hz, and the uncertainty is ±0.5 K.

The pressure transducers are of the strain-gauge type, supplied by Validyne. Positioning around the coolant loop followed three different schemes as illustrated in Figure 2.12, and Appendix A. Manufacturer calibrations were confirmed within an error of ±2 mm H_2O over the full range. Measurements at power-off conditions confirmed these calibrations in situ. Data acquisition was set at 10 Hz.

The electromagnetic flow meter was Model Tigermag 626 made by Sparking Instruments Co., and it was specially compensated to operated at elevated temperatures. The calibration was certified for ±0.36% in the range 0 to 400 gpm (~1.5 m^3/min). data acquisition was set at 10 Hz.

All data were acquired by computer systems, stored, and subsequently analyzed using routines written in MatLab to accommodate specific needs of data processing.

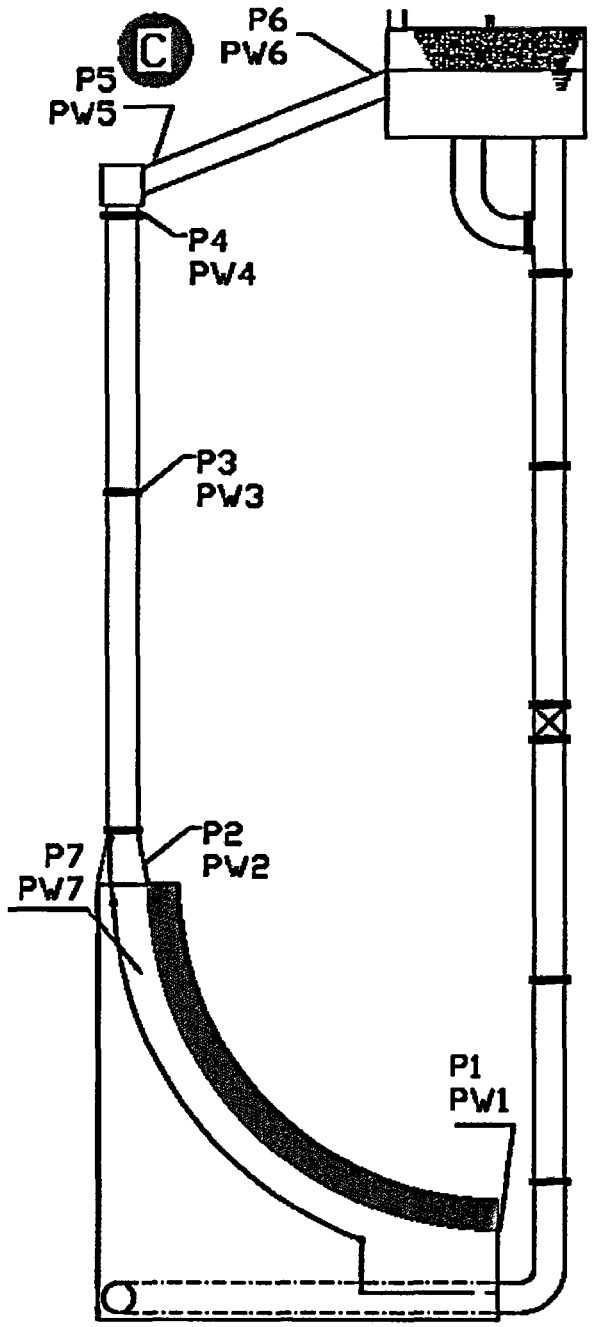

Figure 2.12. Instrumentation scheme (scheme "C").
Positions of thermocouples and pressure transducers.

3. TEST PROGRAM, RESULTS AND INTERPRETATION

3.1 Rationale and main results

The ULPU-V test program is built upon the ULPU-IV program which showed that a notable, enhancement of CHF can be achieved by streamlining the coolant flow path via an improved thermal insulation design. Several key conclusions made on the basis of ULPU-IV data are as follows:

- In the middle (30° – 60°) and lower (0° – 30°) regions we can exceed 1400 kW/m^2 and 900 kW/m^2 respectively; that is, CHF levels are such that, as in the case of AP600, make these regions totally unimportant for IVR performance.

- In the upper region (~75°) we reached the limit of 1880 kW/m^2 without observing burnout.

- At the very top of the heated wall (90°) we found a sudden drop of performance to ~1.6 MW/m^2, and this appears to be related to "exit" phenomena that affect the local two-phase flow structure. It was concluded that this phenomenon needed further study, and remedy.

ULPU-IV results also showed a complex effect of baffle positions (Theofanous et al, 2002a). Note that baffle in the ULPU- IV was made to have a fixed 9" distance to the upper end of the heater surface and a variable distance (from 2½" to 9") to the heater's lowermost region. The ULPU-IV data suggested that the baffle distance to the heater surface in the upper region may be of importance, particularly in addressing the "exit" phenomenon (Figure 3.1). As a result, ULPU Configuration V was designed to allow the baffle position to change in both the upper and lower regions.

The main strategy in performing ULPU-V experimental program was to examine the validity of ULPU-IV findings in Configuration V that reflects AP1000 geometry, to address and overcome the "exit" phenomena found in ULPU-IV tests, and to study other effects of potential importance as found in Theofanous et al (2002b,c). To meet the ULPU-V program objectives, thirty six burnout runs were conducted in three series

- Series M on 6", 3" and 6-to-3" baffle configurations (M6, M3, M63);
- Series C on 3" and 6"-to-3" baffles using de-ionized water on cleansed heaters (C3, C63);
- Series P on 3" and 6"-to-3" baffles using de-ionized water on cleansed heater surfaces with modified power shapes (P3, P63)

The most important results of ULPU-V program can be seen in Figure 3.2. Compared to ULPU-IV CHF data shown on Figure 3.1, ULPU-V CHF data indicate an enhancement, particularly in the uppermost section, where the "exit" phenomena were observed in ULPU-IV test runs.

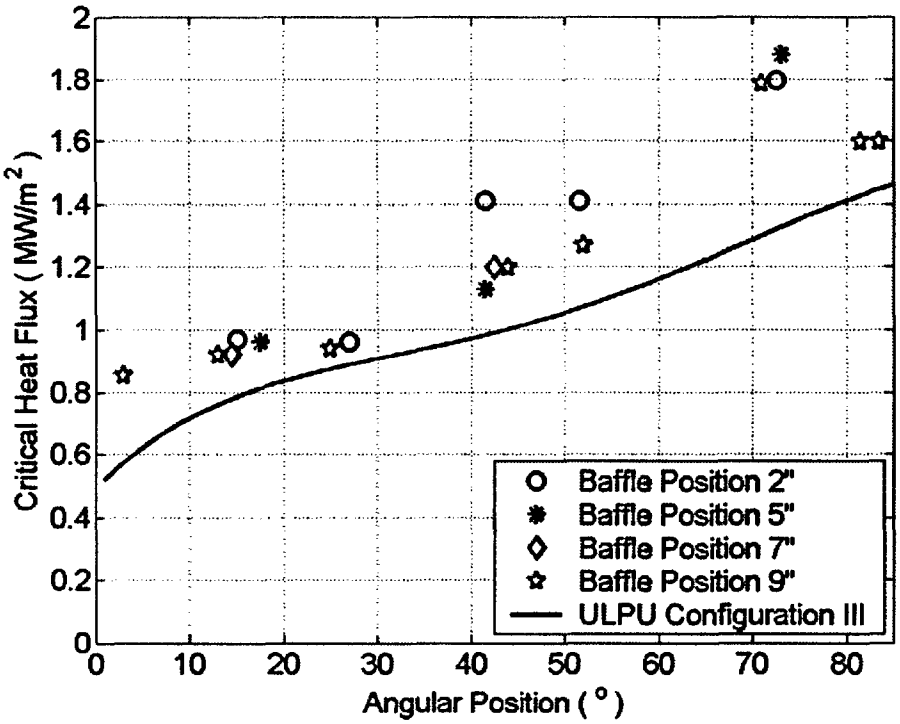

Figure 3.1. Critical Heat Flux measured in ULPU Configuration IV experiments.

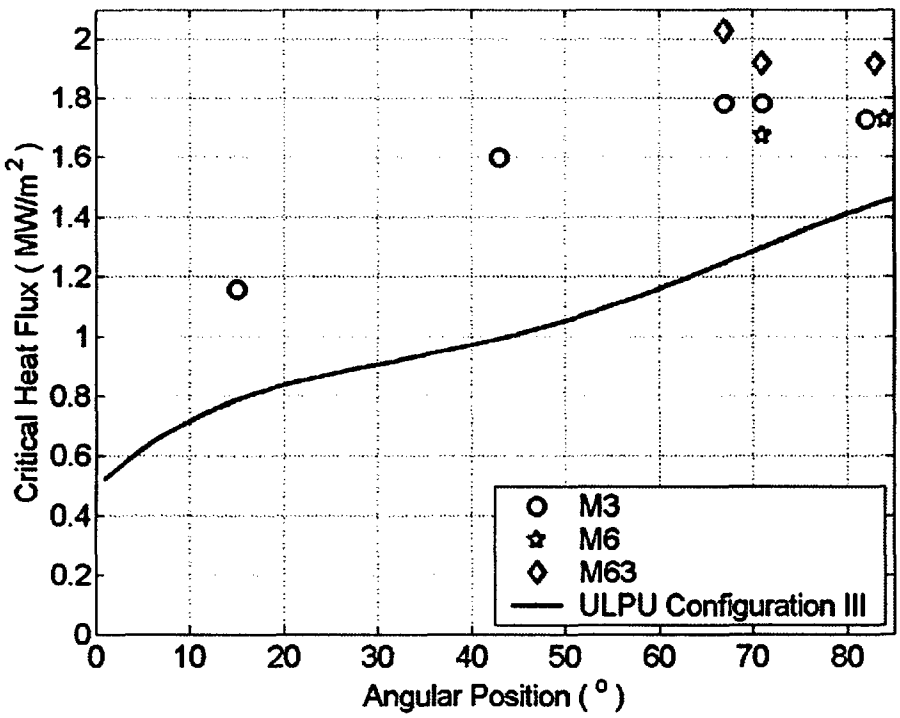

Figure 3.2. Critical Heat Flux measured in ULPU Configuration V experiments.

Detail explanations about test conditions in each series of ULPU-V program are given in respective subsections below. Here we note that the use of de-ionized water in ULPU experiments provides a well-controlled condition for comparison of burnout performance. More importantly, long duration boiling of de-ionized water was found to cleanse the surface of copper heaters that has an apparent effect of water-surface intermolecular interactions and eventually on the limit of coolability in boiling.

3.2 ULPU-V Experiments: Critical Heat Flux in M series

This is the main series of ULPU-V experiments conducted with the objective to examine the validity of ULPU-IV findings for AP1000-specific conditions. A key, and common, characteristic of ULPU-V experiments in the M series is that no cleansing procedure is applied to the heater surface before the burnout testing. This is in the contrary to ULPU-V experiments in C and P series, where de-ionized water was run and boiled for a long duration before the power was increased for CHF measurement.

Specifically, sub-series M6 was run on de-ionized (DI) water shortly after newly sand-blasted copper heaters were installed into ULPU Configuration V facility. It is suggested that strong impact of sand (aluminum oxide) particles used to roughen copper surfaces has also modified surface molecular properties, at least temporarily due to a deposition of aluminum molecules. It is interesting to note that in ULPU-IV experiments, the burnout tests were conducted on de-ionized water. However, the ULPU-IV facility included a section made of aluminum that appears to have served as a source of aluminum oxide deposition on copper heater surface. Therefore, conditions of ULPU-IV tests are closer to conditions of ULPU-V runs in M6 sub-series than ULPU-V experiments in C (or P) series.

Sub-series M3 experiments were also run on DI water, but before the M3 sub-series a tap water boiling treatment was applied to ULPU-V copper heaters. A short boiling process was found to be sufficient to foul the heater surface and modify the surface atomic structure. Finally, the M63 sub-series employed tap water as coolant. Table 3.1 depicts conditions of M series and main results. Detailed results are given in respective sections of Appendix A named according to the run ID number.

Figure 3.2 shows the critical heat fluxes measured in the M series. A significant increase of coolability limit in the lower and medium sections is indicated. More importantly, the ULPU-V M series results are consistent with the ULPU-IV test results. The focus of experiments in M series was naturally placed on the upper section. It can be seen that relative enhancement of critical heat flux in the uppermost location is less than that of the lower angular positions. However, the dramatic reduction observed in ULPU-IV experiments was not found in ULPU-V. An important difference between the ULPU-IV and ULPU-V Configurations with respect to the "exit" phenomenon is that in ULPU-V the channel width in the uppermost section is either 3" (sub-series M3) or 6" (M6 and M63 sub-series), as compared to 9" in ULPU-IV. Notably, the 9" wide channel merged into 6" diameter riser, creating a potential for flow deceleration and even recirculation that negatively affected the

coolability limit. Apparently, a smooth transition from the heater section into the riser in ULPU Configuration V played a positive role.

Table 3.1. Test conditions for runs in ULPU Configuration V - M sub-series.

ID #	Power Shape	Q_{max} Range °	Pre-CHF Flux (kW/m^2)	CHF (kW/m^2)	CHF Position °	Total Power (kW)	Upstream Input Power (kW)	Flow Rate (m^3/min)	Baffler Position (Inch)	Sub-series
	T08A	10~16								
1.			1128	1156	15	345	19	0.689	3	M3
	T24A	38~43								
2.			1504	1598	43	271	71	0.625	3	M3
	T40B	66~71								
3.			1562	1672	71	219	121	0.690	6	M6
4.			1699	1782	71	233	129	0.644	3	M3
5.			1836	1919	71	251	139	0.689	6/3	M63
6.			1974	2028	67	266	147	0.713	6/3	M63
	T40D	66~71								
7.			1754	1782	67	170	129	0.589	3	M3X
	T48A	80~84								
8.			1672	1727	83	205	179	0.693	6	M6
9.			1645	1727	83	207	181	0.645	3	M3
10.			1782	1919	83	230	201	0.675	6/3	M63

Figure 3.2. Critical Heat Fluxes as measured in ULPU-V test program.

Still within the M series we observe certain differences between CHF values measured in M3, M6 and M63 sub-series. Possibly, these differences originated from waters and surface treatments applied in these sub-series. Relatively lower CHF in M6 sub-series compared to M63 sub-series is likely related to the use of de-ionized water and tap water in the two respective test series. Furthermore, M6 run #8 was conducted after M6 run #3, so that the molecular deposition of aluminum may have partially been dissolved by de-ionized water used in the M6 experiments. Significantly reduced CHF measured in subsequent experiments (~ 1300 kW/m^2) pointed to a degradation effect, when removal of a surface deposition layer is completed. A similar behavior due to heater surface modification in DI water may have occurred in the M3 test series. Time sequence of M3 runs #1, #2, #4, #7 and #9 pointed to a possible cleansing of an initial surface modification (deposition) applied before M3 run #1.

Experiments in ULPU-V M63 sub-series on tap water showed highest values of CHF that exceeded 1.8 MW/m^2 even in the heater's uppermost region. The time sequence of M63 runs was #5, #6, and #10. It should be noted that boiling processes in the M63 runs lasted for six hours, ensuring a steady state in each power level. However, for clarity and consistency of data representation in Appendix C, power and temperature histories of the M63 runs are given for the typical duration of three minutes for each power level. Therefore, the time

shown in these power and temperature histories represents snapshots rather than the complete physical time history. Detail examination of temperature measurements in the M63 runs shows that the heater temperature continued to increase during the boiling process. It is because of the increasing thermal resistance due to a thickening layer of foul deposition from tap water. While such a foul layer was found to enhance the coolability limit, the added thermal resistance caused overheating in ULPU heaters. In prototypic reactor conditions, containment water contains boric acid and trisodium phosphate which have different chemical and solubility behaviors than chemicals present in tap water. The effect of containment water chemistry on burnout is examined in separate tests on BETA and presented in section 4.

3.3. ULPU-V Experiments: Critical Heat Flux in C series and P series

Both C and P series were designed to measure critical heat flux under conditions when copper heater surface had undergone a cleansing procedure by extensive boiling in DI water. The purpose of such a surface treatment is to rid the copper surface from molecular modifications, either due to an initial sand-blasting procedure or due to tap-water deposition. Such a surface treatment was possible in ULPU-V because of the use of stainless steel to replace aluminum details in ULPU construction. Remarkably, we observed the ULPU-V copper surface becoming shin and clean after a long duration boiling of DI water. Apparently, well-known to be aggressive, DI water promoted dissolution of oxidic compounds deposited on the heater surface.

Another objective of experiments in C and P series is to enlarge the database to uncover factors that may have influenced the limit of coolability in ULPU experiments. Toward this end, modified power profiles were used in P series to achieve an increase of heat flux in the region upstream of burnout location being tested. The resulting input power upstream the designated burnout location is made to increase 20% in T40E and T48B, and 40% in T40F and T48C, compared to standard power profiles (T40B and T48A, respectively) used in M and C series (see Figures 2.10-2.11).

Table 3.2 shows test conditions and main results of CHF experiments in C series and P series. Compared to M series test results, C and P series experiments gave significantly reduced values of CHF. Clearly, the limit of coolability is dominated by characteristics of heater surface. While the governing effect of surface aging on phenomena of boiling crisis was examined in our previous study of pool boiling on flat plate (Theofanous et al, 2002ab), ULPU-V experiments show, for the first time, a surface control of burnout in such large-scale, flow boiling situations.

Quantitatively, Figure 3.3a depicts critical heat flux measured in C and P sub-series at angular positions from 66° to 84° as a function of parameter x at the burnout location, where $x = Q_{PRE}/G.H_{LV}$ (Q_{PRE} [kW] is the input power in the heater region upstream of the location of maximum heat flux; G [kg/s] is coolant mass flow rate, and H_{LV} [kJ/kg] is the latent heat of evaporation). In this definition, "x" is "atmospheric" equilibrium vapor mass quality in the flow channel when the local subcooling due to over-pressure is not taken into account. It can

be seen that CHF data from P series provide the lower bound of 1.3 MW/m^2. Within the range of "x" tested, no distinguishable trend can be discerned.

Table 3.2. Test conditions for runs in C and P series.

ID #	Power Shape	Q_{max} Range °	Pre-CHF Flux (kW/m^2)	CHF (kW/m^2)	CHF Position °	Total Power (kW)	Upstream Input Power (kW)	Flow Rate (m^3/min)	Baffle Position (Inch)	Sub-Series
	T08A	10~16								
11.			916	987	10	309	17	0.654	3	C3
12.			902	930	83	265	265	0.696	6/3	C3
	T24A	38~43								
13.			940	1128	46	191	50	0.625	6/3	C63
	T40B	66~71								
14.			1645	1672	71	219	121	0.608	3	C3
15.			1233	1507	71	198	109	0.556	3	C3
16.			1370	1453	71	190	105	0.649	6/3	C63
17.			1370	1425	71	187	103	0.658	6/3	C63
	T40D	66~71								
18.			1425	1480	67	170	129	0.590	3	P3X
	T40E	66~71								
19.			1288	1343	71	196	117	0.681	3	P3
20.			1343	1398	71	204	122	0.684	3	P3
21.			1233	1370	71	200	120	0.671	3	P3
22.			1233	1370	67	198	120	0.633	6/3	P63
	T40F	66~71								
23.			1316	1370	71	243	162	0.690	3	P3
24.			1233	1316	71	233	156	0.693	6/3	P63
	T48A	80~84								
25.			1238	1507	80	179	156	0.656	3	C3
26.			1370	1480	83	178	155	0.679	3	C3
27.			1233	1370	83	165	144	0.572	3	C3
28.			1370	1507	80	181	158	0.601	6/3	C63
29.			1398	1453	83	175	152	0.633	6/3	C63
30.			1370	1507	83	181	158	0.611	6/3	C63
	T48B	80~84								
31.			1288	1343	83	209	188	0.677	3	P3
32.			1233	1288	80	200	180	0.650	3	P3
33.			1233	1370	83	213	192	0.657	3	P3
34.			1233	1370	83	213	192	0.666	6/3	P63
	T48C	80~84								
35.			1261	1288	80	238	228	0.692	3	P3
36.			1233	1370	83	253	242	0.685	6/3	P63

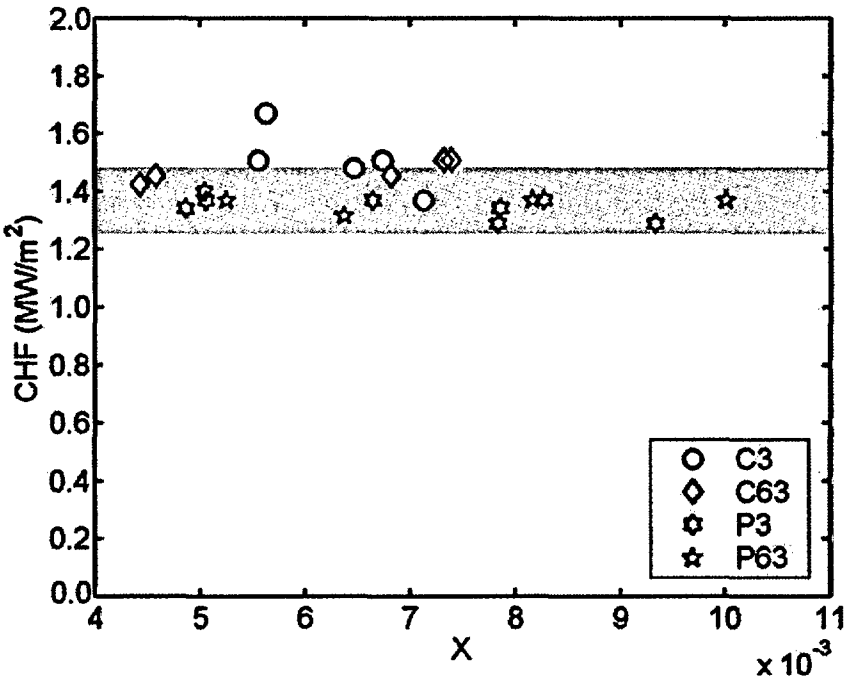

Figure 3.3a. Critical Heat Fluxes measured in ULPU-V C and P sub-series for $66° < \theta < 90°$ *as function of quality x determined as* $x = Q_{PRE}/G.H_{LV}$*, where* Q_{PRE} *[kW] is the input power in the heater region upstream of the location of maximum heat flux; G [kg/s] is coolant mass flow rate, and* H_{LV} *is the latent heat of evaporation (kJ/kg). Shaded area shows CHF range in ULPU-III for AP600.*

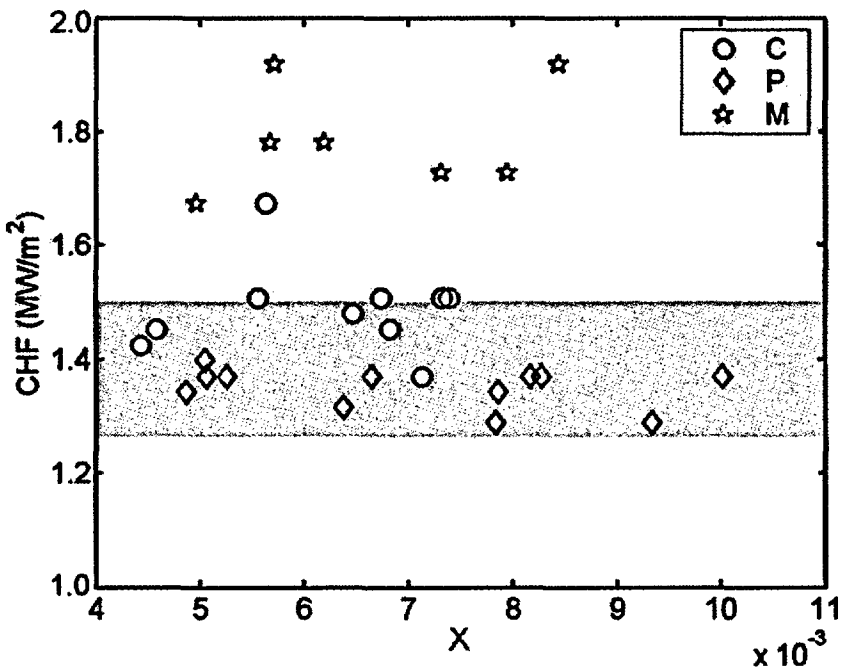

Figure 3.3b. ULPU-V CHF for $66° < \theta < 90°$ *as function of x (see caption Figure 3.3a). Shaded area shows CHF range in ULPU-III for AP600.*

Furthermore, we note that, for the same range of angular positions, equilibrium vapor mass quality at the burnout location in M sub-series also varies in a similar range as in C and P sub-series, but the CHF values are clearly higher (Figure 3.3b). It is remarkable because the observation indicates that not the local flow enthalpy determined by input power, but heater surface and water quality hold the first-order key to burnout in the upper region.

However, CHF under ULPU conditions is not totally a local phenomenon as can be seen from comparison results of C and P sub-series. CHF measured in P sub-series (1300-1350 kW/m^2) are ~100-150 kW/m^2 lower than CHF measured for corresponding tests in C series. Notably, burnout occurred in P series at lower heat fluxes but at larger input power upstream of the burnout location, larger total input power and higher flow rates (see Table 3.2).

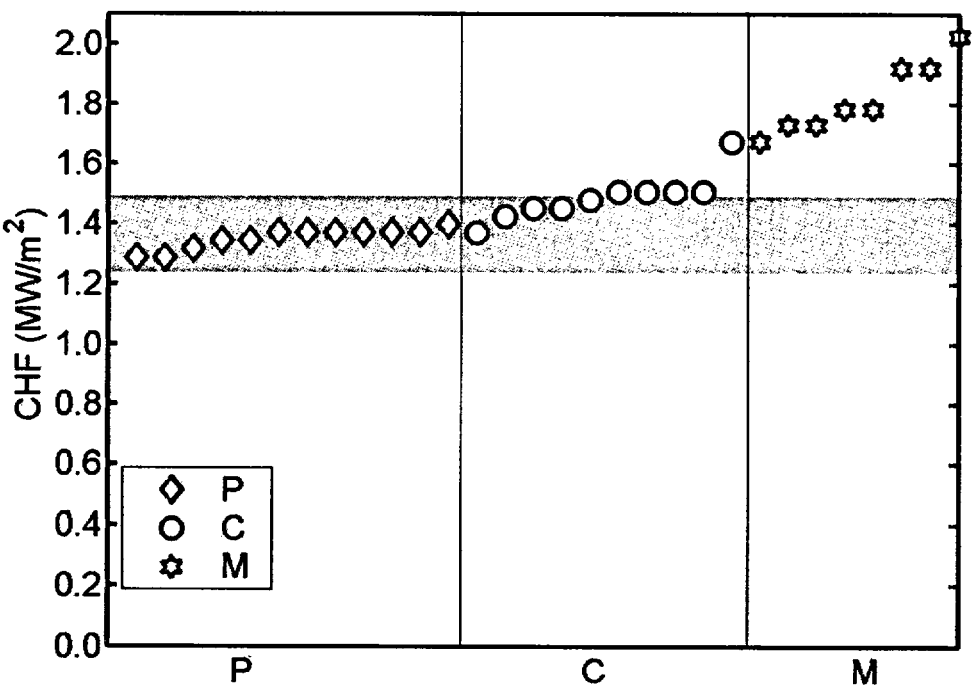

Figure 3.4. Critical Heat Fluxes as measured in ULPU-V for 66° < θ < 90°. The shaded region shows CHF range obtained in ULPU Configuration III for AP600.

3.4. Flow rate and pressure data

For each experimental run, measured flow and pressure data are given in Appendix C and an explanation of data type is given in Appendix B. Note the 10 Hz frequency of data acquisition for pressure and flow rate. Subsequent analysis shows that the 10 Hz acquisition rate is sufficient to capture all pressure variations in ULPU-V. Also, schematic of instrumentation locations is given in Appendix A. For example, differential pressures ΔP_{12}, ΔP_{23}, ΔP_{34}, ΔP_{45}, and ΔP_{56} correspond to sections in ULPU-V facility

- section 12: heated channel;
- sections 23 and 34: lower and upper section of the riser;
- section 45: transition exit from riser to inclined channel;
- section 56: inclined channel merged into the upper tank (see Fig.2.2).

It should be noted that experimental data on pressures and flow rates are highly reproducible in different tests when similar power profiles are used (see, for examples, results of runs #16 and #17, runs #28, #29 and #30). The reproducibility is paramount in such complex two-phase flow regimes as they occur in ULPU experiments, showing a robust behavior of two-phase natural circulation in ULPU-V loop. Interestingly, similar results of flow rates and pressure losses were measured in tests with 3" baffle and 6-to3" baffle configurations with the same power profile (e.g., see #35 and 36). This observation can be important in considering the effect of slice representation of vessel lower head in ULPU.

Flow rates

Figure 3.5 shows flow rates as function of total input power. It is natural to expect that with the increase of input power, the increased coolant enthalpy would lead to higher void fraction in the riser and therefore larger driving force for natural circulation flow. That is to say, the flow rate is expected to increase with the input power. Such an increase can be seen in Figure 3.5 for the range of input power in ULPU-V runs. Remarkably, ULPU-V data showed a weak dependence of natural circulation flow rate on input power, changing from 0.5 m^3/min to 0.7 m^3/min for the input power range from 100 kW to 350 kW. The natural circulation flow rates at burnout power level are in even a narrower range around 0.6-0.65 m^3/min (Figure 3.6a-3.6b). The flow rate of 0.6 m^3/min can be translated into 50...55 m^3/min (or ~14500 gpm) in a prototypic AP1000 reactor condition. Interestingly, sorting of the flow rate data by CHF run series (C, P and M) as shown in Figure 3.6a and by baffle positions (3", 6" and 6"-to-3") as shown in Figure 3.6b did not reveal any stratification of data.

Figures 3.7a-b show flow rates as a function of critical heat flux measured in ULPU-V experiments. It is remarkable that the flow rate at burnout remains nearly unchanged for CHF range from 1 MW/m^2 to 2 MW/m^2. Again, no CHF data stratification was found.

Measured flow rates can be understood better from the analysis of pressure drops in highly non-equilibrium two-phase flow natural circulation loop in ULPU. While pressure drop data are given shortly below, we note two-phase flow regimes in ULPU are largely governed by boiling/condensing phenomena in subcooled flow. On one hand, vapor mass

quality and volume fraction at the entry into the upper tank (point 6, Fig.2.12) can be estimated on a equilibrium basis as

$$x = q/(m \,.\, H_{LV}) = 250\ (kW)/(10\ kg/s)/(2257\ kJ/kg) \cong 0.01$$

$$\alpha = [1 + S * \rho_V/\rho_L * (1-x)/x]^{-1} = 0.61\ (\text{slip coefficient } S=10)$$

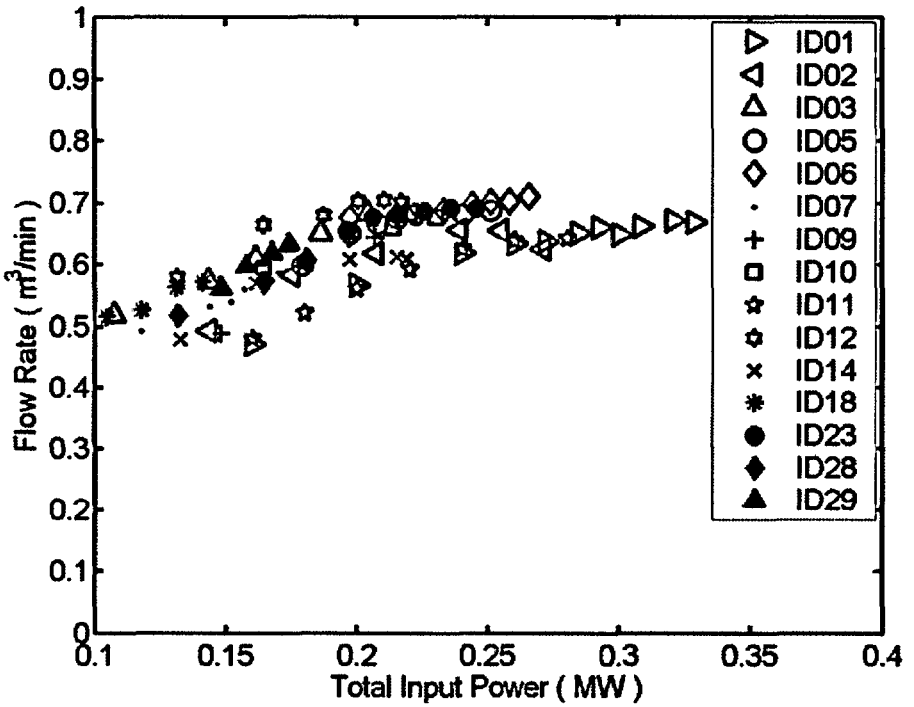

Figure 3.5. Flow rate as function of input power (data at different power levels).

However, heater blocks in ULPU are well under the water free surface level, 4.8 (min) to 6.2 m (max). These elevations correspond to 0.45 bar and 0.58 bar of overpressure, or water saturation temperature at 113K and 110 K. Given the water at the upper tank being saturated at atmospheric pressure and negligible heat loss (less than 1 kW in a 200 kW device), water subcoolings ΔT_{SUB} at the heater blocks are evaluated as 10 K and 13 K. In a well-mixed condition, a typical coolant flow rate at G = 0.62 m^3/min (≅165 gpm ≅ 10 kg/s) requires an input power of

$$Q_{SUBCOOL} = G * C_p * \Delta T_{SUB} = 10\ (kg/s) * 4.2(kJ/kg.K) * 10\ (K) = 420\ kW$$

to compensate for the 10 K subcooling. This value of $Q_{SUBCOOL}$ can be appreciated in light of typical input power in ULPU-V at the level of 250 kW. Therefore, subcooled boiling is dominant regime in the heated section 12. Beyond the upper boundary of ULPU heated blocks, steam rapidly condenses and coolant flow in the riser section 23 becomes essentially single-phase liquid. The coolant boil-off re-emerges at higher elevations in section 34 and two-phase flow dominates in section 45 and 56. Void fractions in these upper sections are the

driving force for natural circulation, which is balanced by friction losses which are also largest in these two-phase regions.

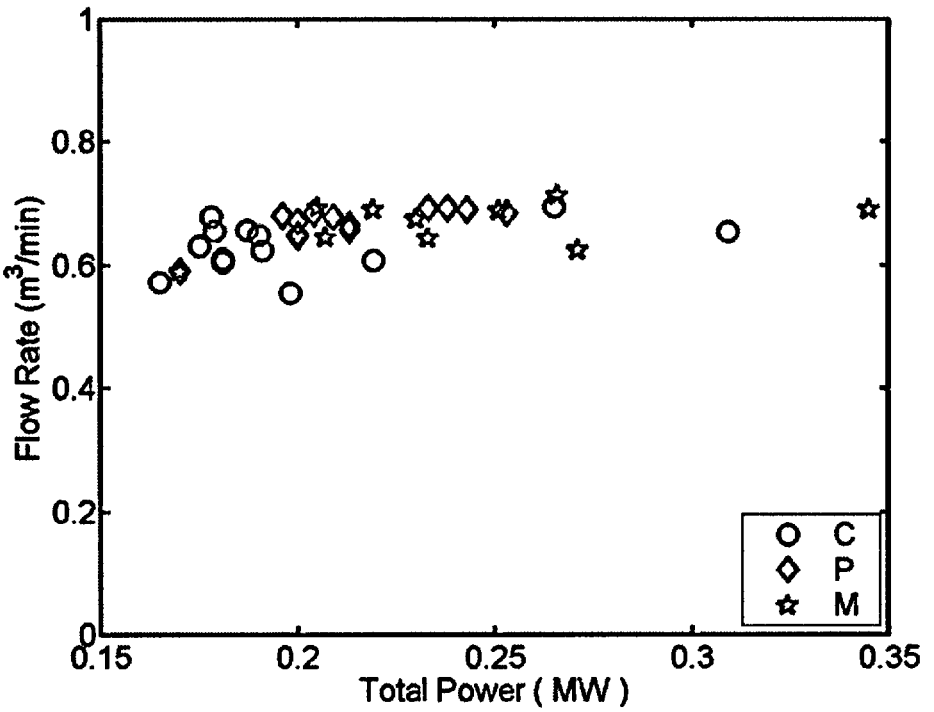

Figure 3.6a. Flow rate as function of input power (data at burnout level, sorted by test series).

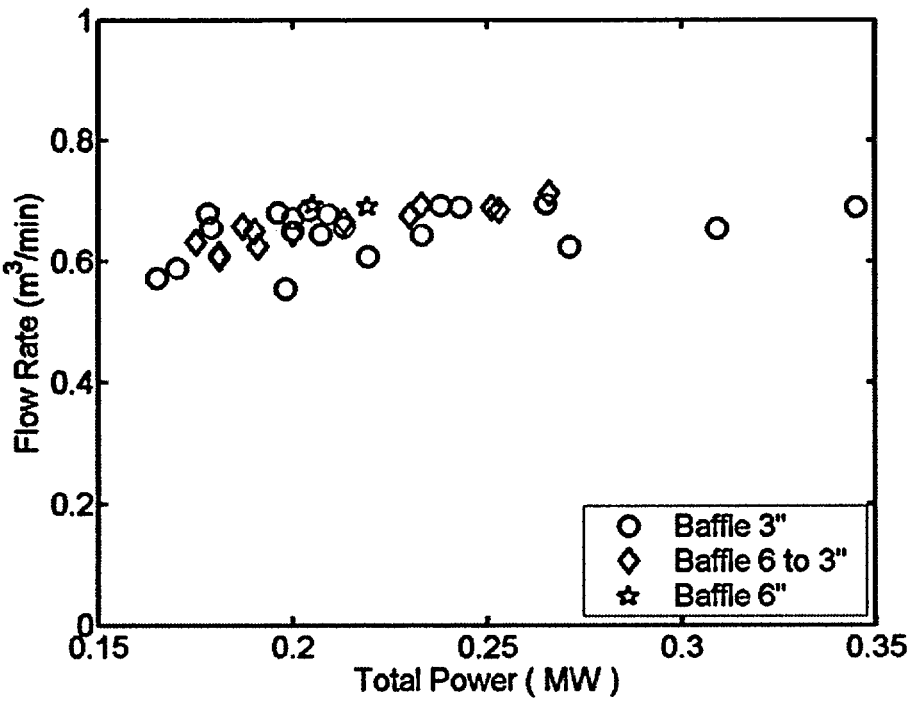

Figure 3.6b. Flow rate as function of input power (data at burnout level, sorted by baffle position).

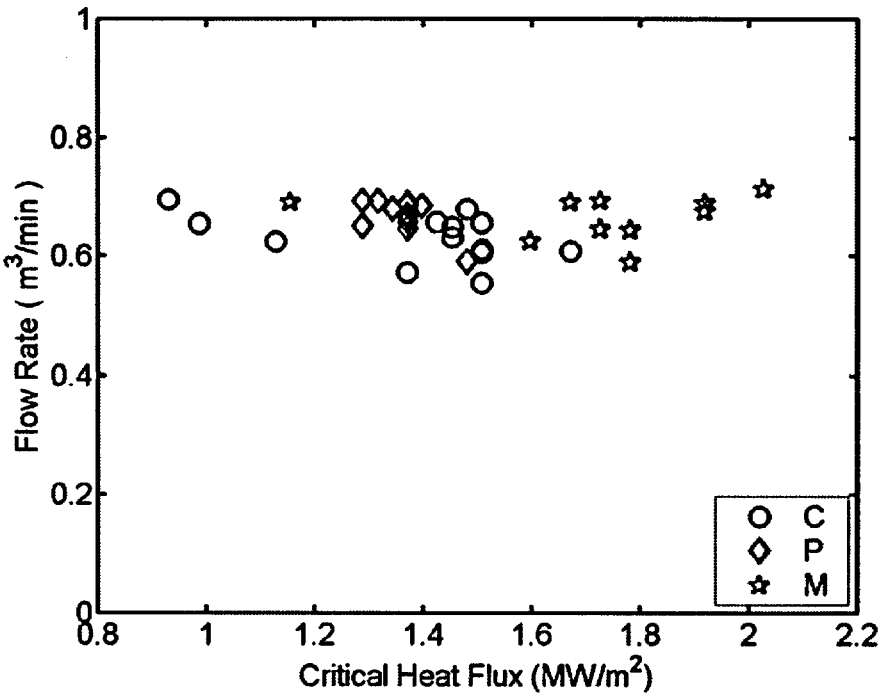

Figure 3.7a. Flow rate as function of input power (data at burnout level, sorted by test series).

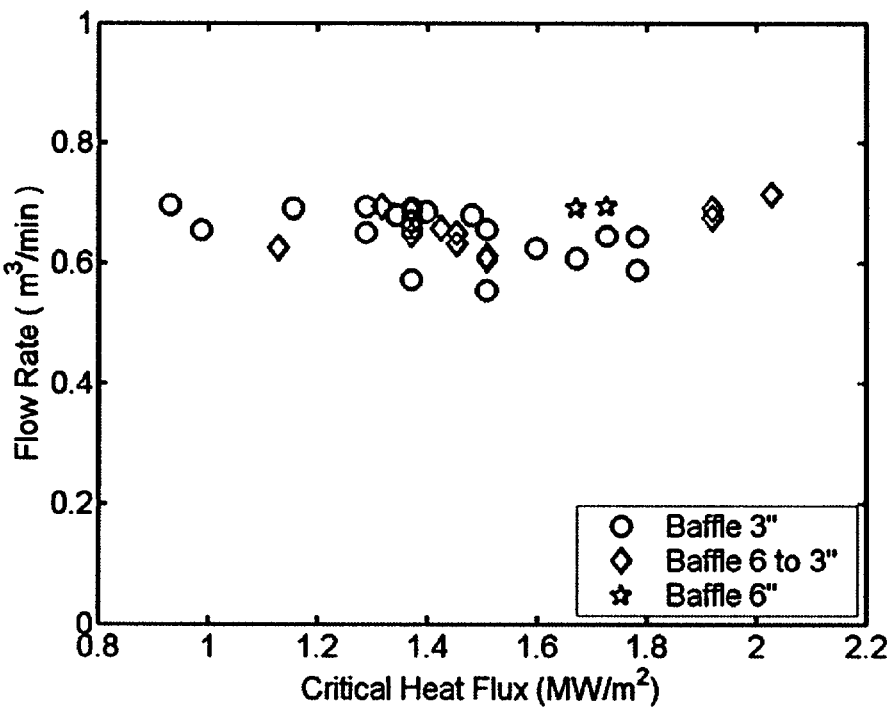

Figure 3.7b. Flow rate as function of input power (data at burnout level, sorted by baffle position).

Pressure drops in natural circulation loop

Figure 3.8 depicts pressure drops in different sections in the uprising branch of ULPU-V natural circulation loop as function of flow rate. Test runs with a broad range of flow rate variation were selected for presentation in this figure, so as to reveal a trend in data correlation between pressure drops and flow rates. Both flow rates and pressure drops were averaged values calculated for a sufficiently long duration of quasi steady state.From the results just presented the flow rate coordinate in Figure 3.8 can be readily translated to total input power.

The behavior seen is straightforward. At low power levels pressure drop differentials measured correspond to respective gravity heads. Section 56, the inclined pipe is the first to experience the presence of voids as power increases to produce flow rates of over 0.5 m^3/min. The seen reduction of gravity head ultimately levels out with power (flow) as significant voids develop in this pipe to allow slip. This is on the top, where the water has to come to equilibrium at atmospheric pressure by flashing, and it is here that the gravity head that initiates two-phase natural circulation originates.

The next section to contribute to the gravity head that drives this flow is the heated channel itself (section 12). Non-equilibrium voids develop here, and they even slightly penetrate upwards into section 23 at the upper end of the power (flow) range. Otherwise this section 23 remains subcooled and single phase, as already expected from the power estimates above. Next to contribute is the top of section 34, as the flashing front from above (the inclined pipe) penetrates periodically downwards, in an manner that allows more flashing to occur below as water boils 9and is carried away) from above. The depth of this penetration is controlled by the water temperature in section 23, and by the increased acceleration and frictional pressure drop that develops with flashing two-phase flow going through the nozzle restriction (section 45). Thus, this is the ultimate mechanism that controls the magnitude of the time-average flow rate. This significantly higher pressure drop requirement is seen in Figure 3.8d, indeed, the only section that exhibits a pressure drop increase.

Evidently the mechanism that controls flow is an intricate balance between non-equilibrium (in the heater section 12) and flashing-dominated (at the upper end) gravity heads on one hand and acceleration/frictional losses in the complex nozzle geometry on the other. While not amenable to a priori prediction, the nature of the loss component is such that it would be likely overestimated in our small scale simulation of the nozzle gallery, and thus we can expect that the reactor would exhibit higher natural circulation flow rates than obtained in our tests.

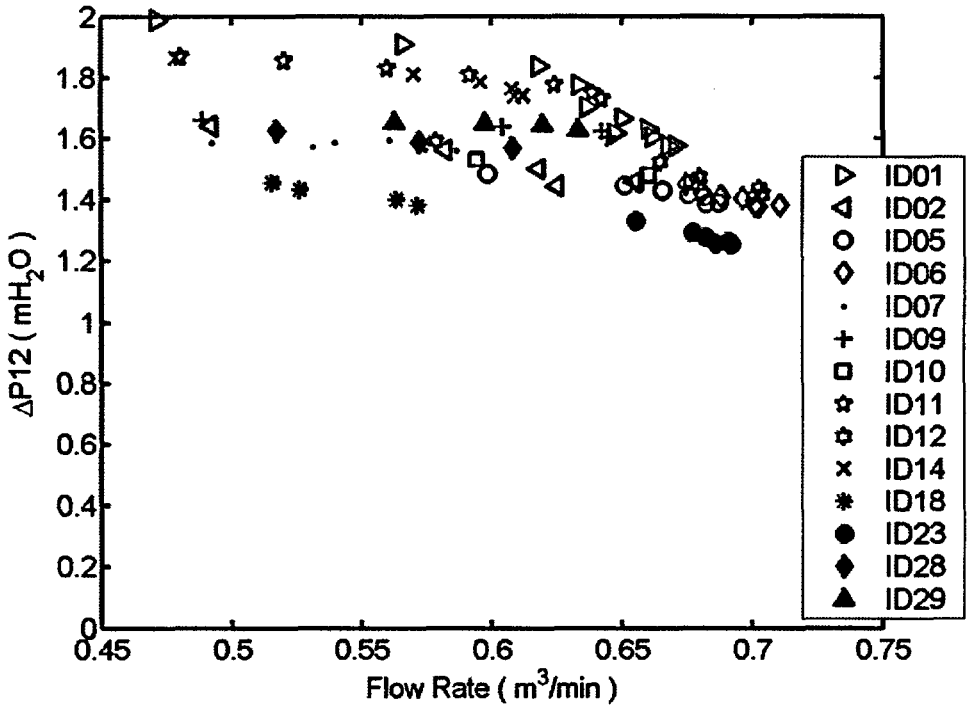

Figure 3.8a. Pressure drop over section 12 (heated channel around the vessel lower head, H_{12} *= 1.75 m)*

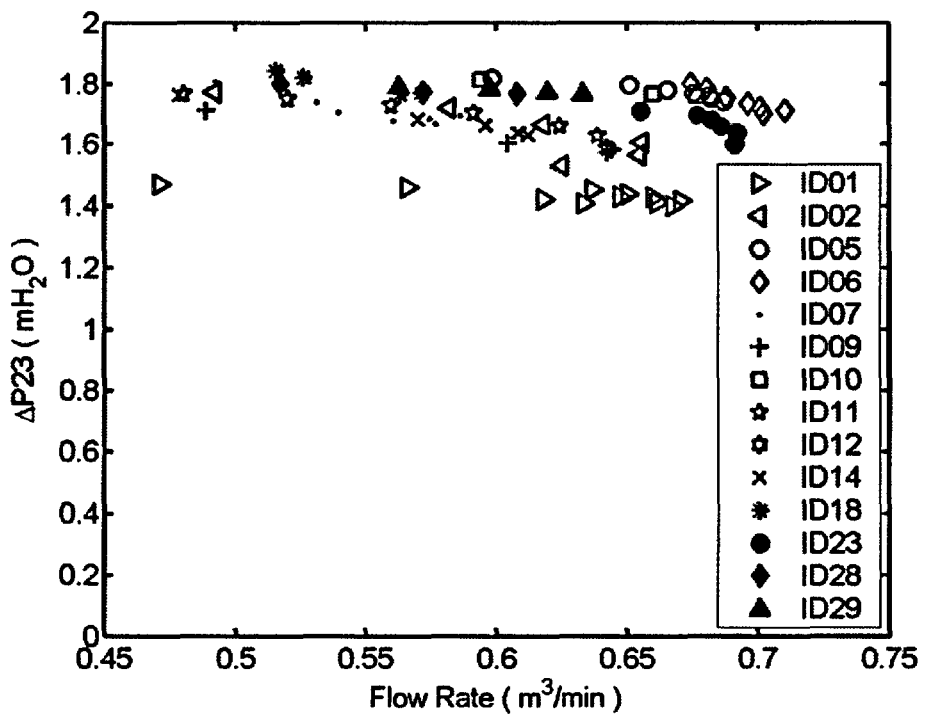

Figure 3.8b. Pressure drop over section 23 (riser's lower region, H_{23} *= 1.85 m).*

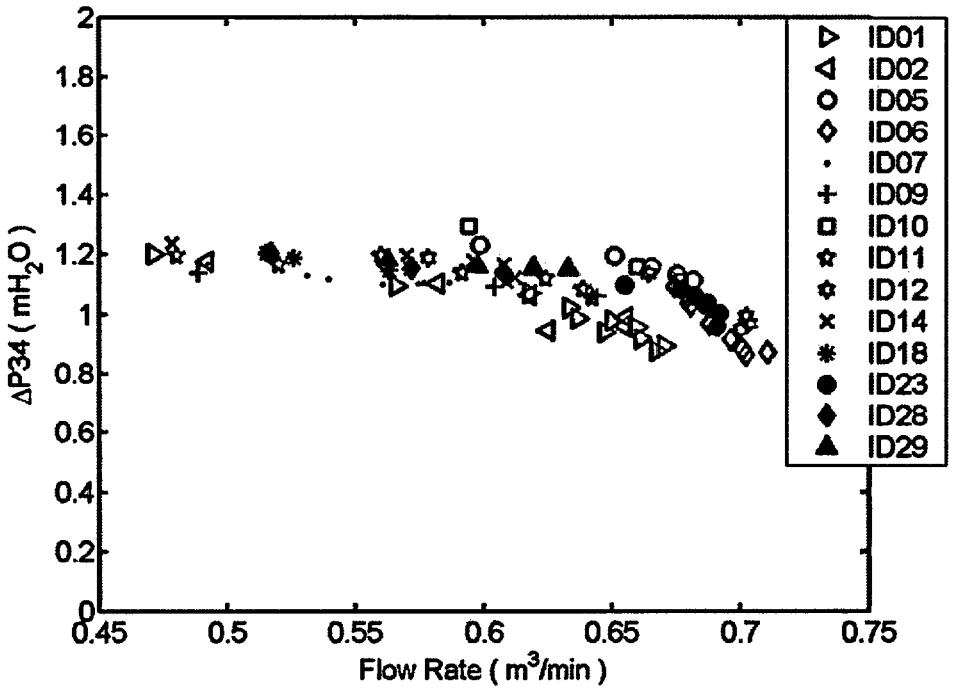

Figure 3.8c. Pressure drop over section 34 (riser's upper region, H_{34} = 1.25 m).

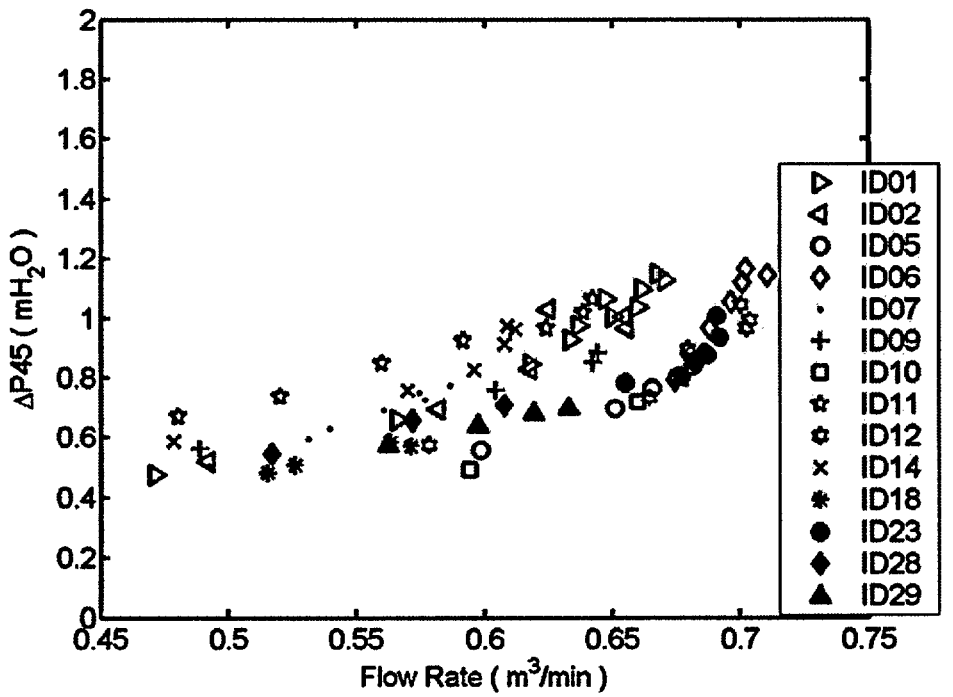

Figure 3.8d. Pressure drop over section 45 (riser's exit – nozzle, H_{45} = 0.4 m).

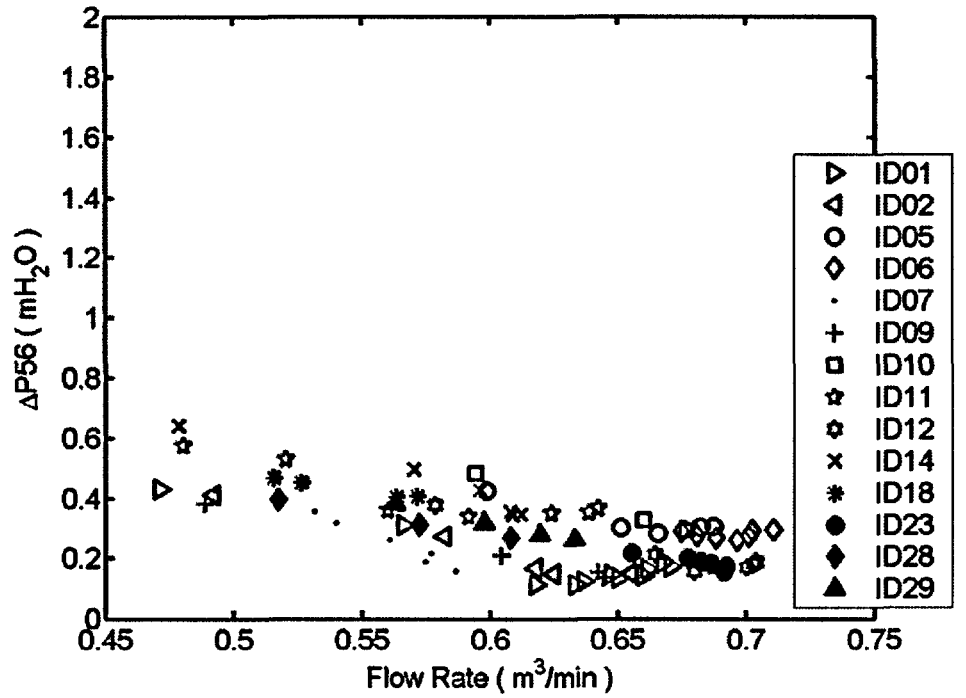

Figure 3.8e. Pressure drop over section 56 (inclined pipe, H_{56} = 0.65 m).

Pressure time series and fast Fourier transform.

Figure 3.9 shows original pressure data as measured by different pressure transducers in a typical run. Regular oscillations of ±0.2 m with 5 s periods can be seen in pressure data for P3, P4 and P5. Measured pressure data are shown in Appendix C for each test run over the whole run duration. Of interest are pressure transients in response to changes of input power that affect evaporation, hydraulic heads and natural circulation flow rate in ULPU-V.

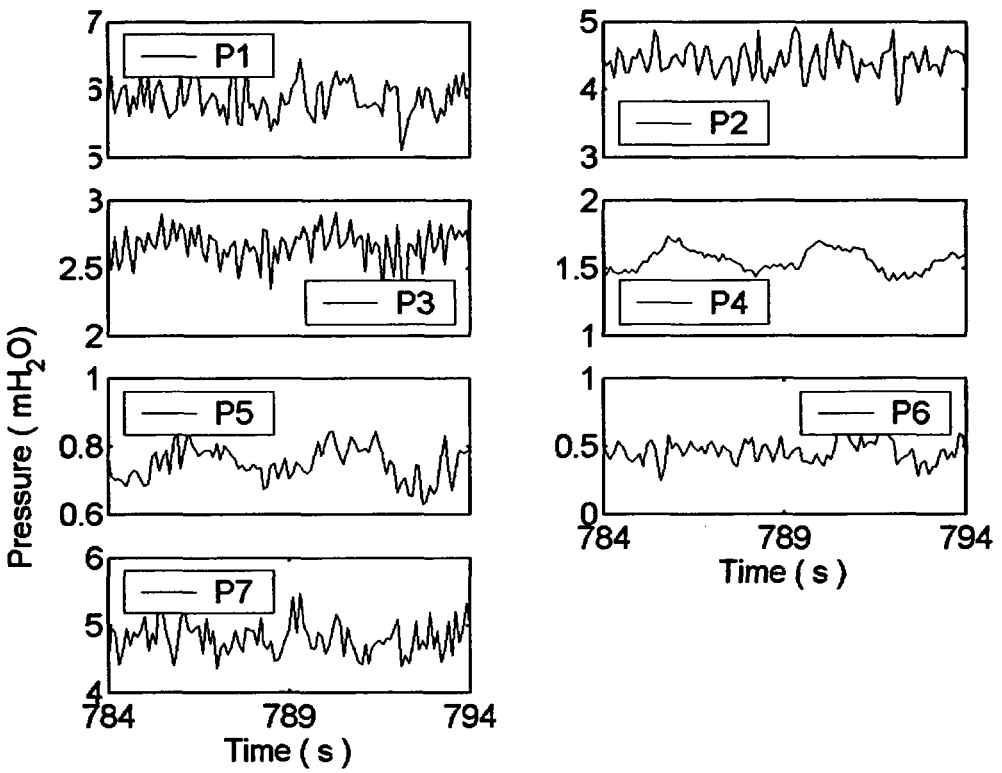

Figure 3.9. Original pressure data (run #10)

Figure 3.10 depicts power spectra of pressure as obtained from Fast Fourier Transform (FFT) for four cases, at the highest power level of selected runs. Notably, we found no distinct differences in power spectra in runs with different baffle configurations or power shapes. It can be seen in Figure 3.10 that in all cases pressure oscillations are defined sharply at frequency around of 0.2 Hz and they are present in all locations of the system (Figure 3.10a-b). Other higher-frequency pressure fluctuations are found to dominate in the region around the vessel lower head. These higher frequency fluctuations may vary in a narrow range around 1 Hz at one extreme as shown in Figure 3.10c, or spread over a wide range from 0.5 Hz to 2 Hz and higher at the other extreme . It is noted that these high frequency fluctuations have the highest amplitude, ±0.5 m of water column, and they must be taken into account in the structural design of the thermal insulation. At the root of these pressure oscillations are non-equilibrium nature of two-phase flow in the downward facing heated configuration, with intense evaporation and condensation due to liquid subcooling.

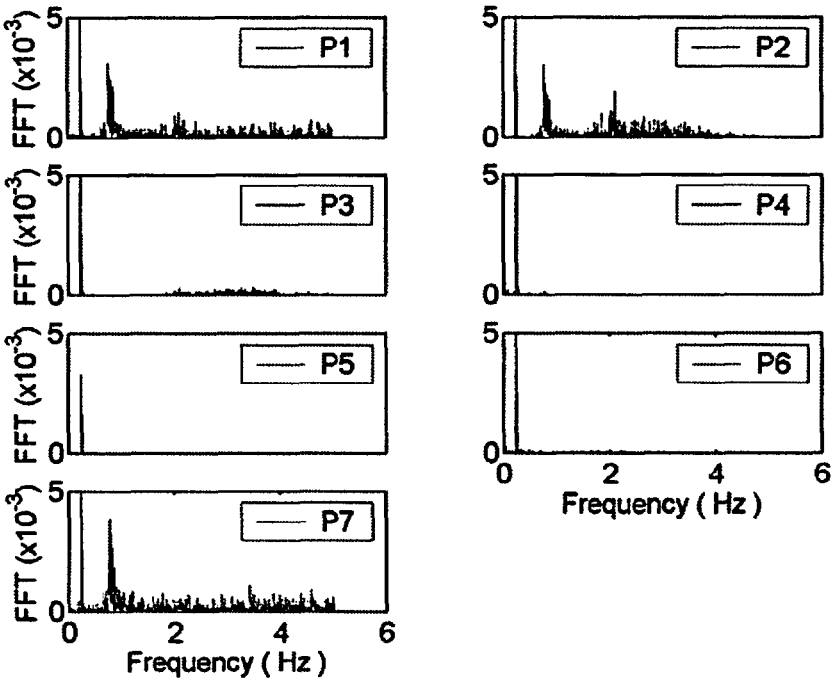

Figure 3.10.a. Fast Fourier Transform spectra of pressure data (run # 10, M63, 230kW).

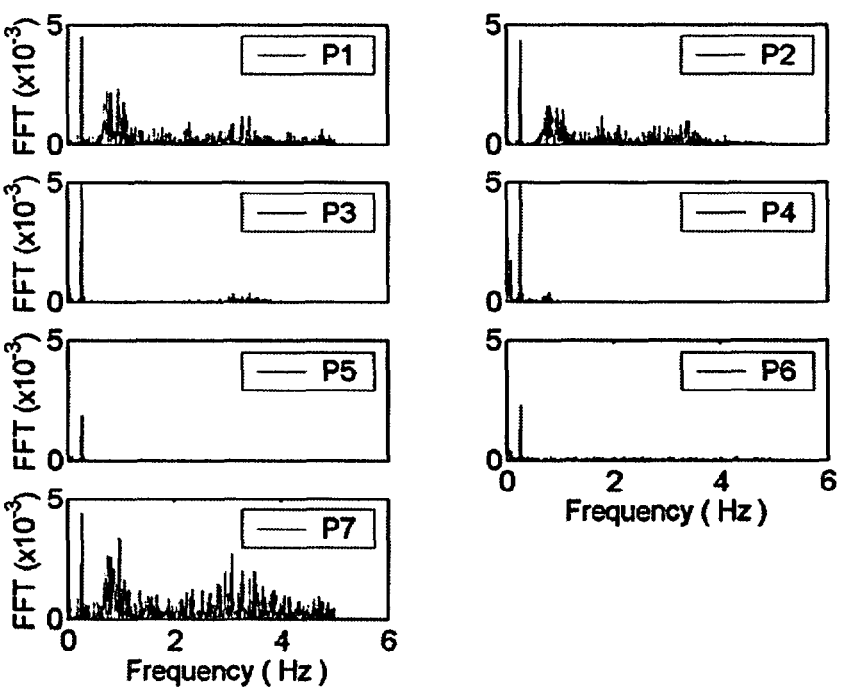

Figure 3.10.b. Fast Fourier Transform spectra of pressure data (run # 6, M63, 266kW)

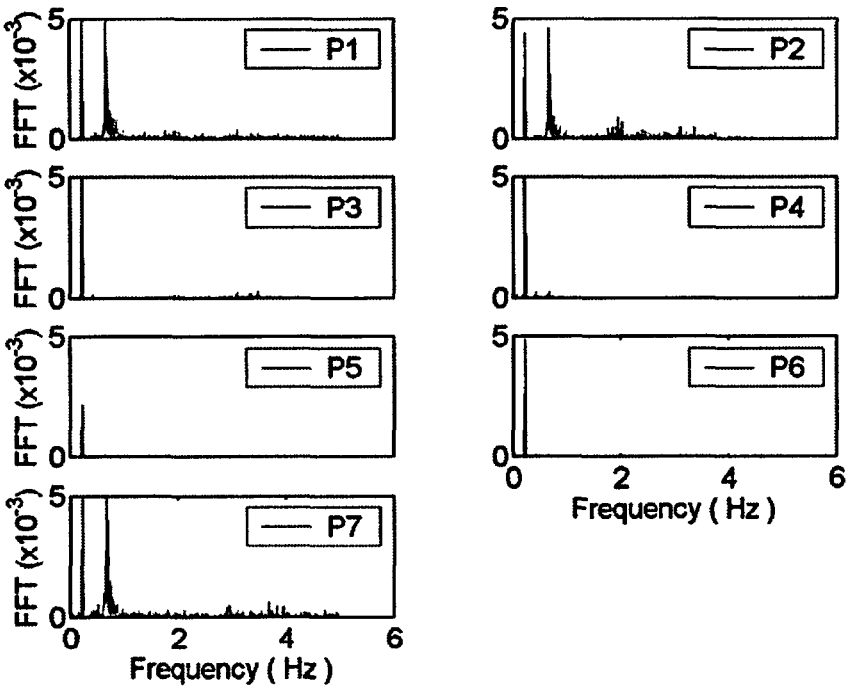

Figure 3.10.c. Fast Fourier Transform spectra of pressure data (run #17, C63, 187kW).

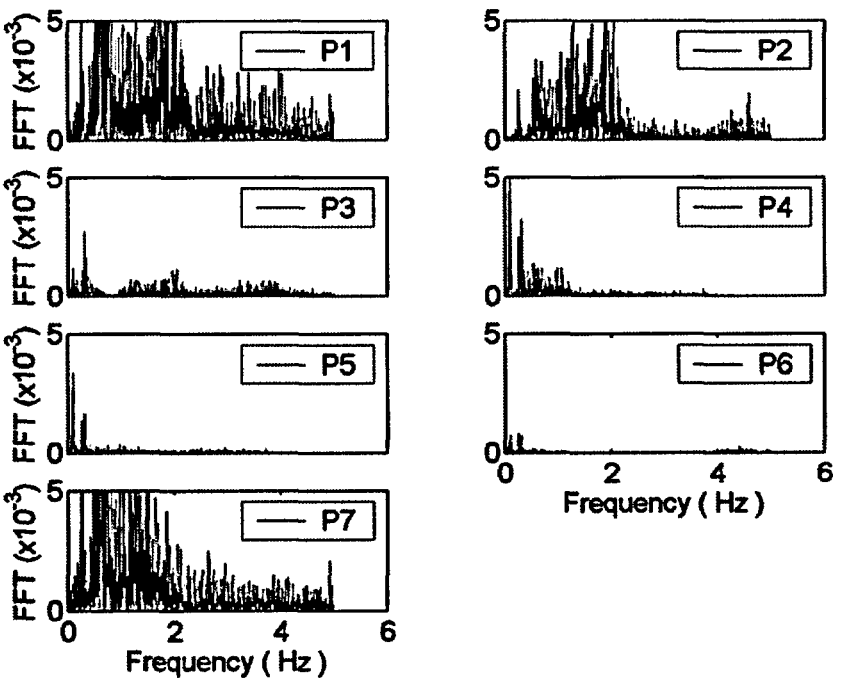

Figure 3.10.d. Fast Fourier Transform spectra of pressure data (run #3, M3, 345 kW).

4. SUPPORTING SEPARATE-EFFECTS (BETA) EXPERIMENTS

Results of ULPU-V experiments presented in Section 3 show a significant effect of water chemistry and surface conditions on critical heat fluxes (see also Theofanous et al, 2002b-c). Notably, CHF values measured in series C and P are 50% lower than CHF measured in M series. Also, in preliminary BETA tests (not reported here) we found that typical paints and coating used to protect the reactor vessel during shipping (and normally left on it during operation) can have detrimental effects on CHF performance. Thus we recommended that in AP1000 such a protective layer is strippable, and that it be removed during installation, leaving bare steel as the surface of interest under IVR. Here, we focus on the effect of chemicals, expected to be present in containment waters, namely Tri-Sodium Phosphate (TSP) and Boric Acid (BA). The base condition is pure, deionized water. Besides bare prototypical steel surfaces, copper surfaces are examined as well, so as to connect with the heater block surfaces in ULPU.

4.1. BETA experimental program

We use cartridge heaters embedded in a 5-cm-thick copper block to provide the required input power. Figure 4.1 depicts a schematic of BETA test section, which is self-explanatory. The power supply is regulated and monitored (±5%) by a computerized control system not shown in Figure 4.1.

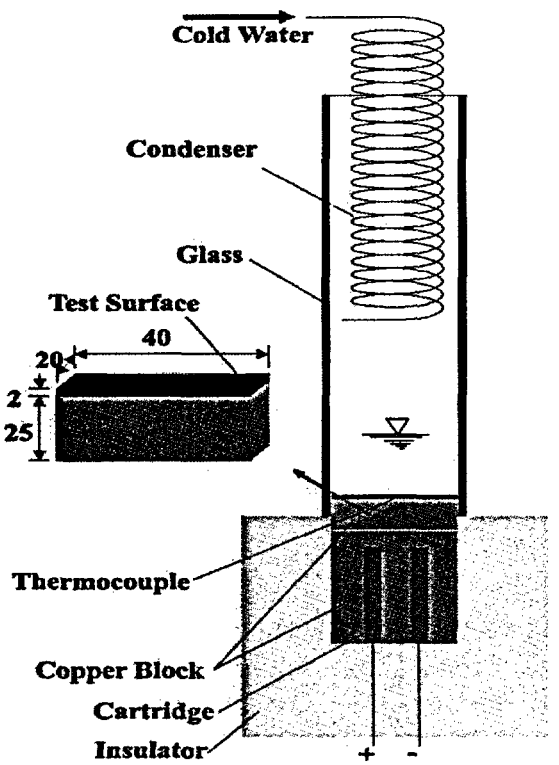

Figure 4.1. BETA-C and BETA-S experimental test section. All dimensions in millimeter.

Specifically, the cartridge heaters have maximum power up to 1 kW each, sufficient to provide a surface heat flux of up to 2.5 MW/m^2 which is quite adequate for these pool boiling experiments. The heat transfer area is 20x40 mm, large enough to provide one-dimensional behavior of pool boiling as discussed and demonstrated in Theofanous et al (2002a-b).

In copper heater experiments, BETA-C series, the copper block itself provides the heat-transfer surface. The surface is sand-blasted prior to each series of experiments. Similar sand-blasting technology was used for treatment of copper blocks before their installation in ULPU-V facility. No other coating is used to allow the copper surface to age and modify in boiling.

In steel heater experiments, BETA-S series, a 2mm-thick steel piece is attached to the copper block by a process (silver soldering) that ensures good, stable contact, and has minimal effect on the steel surface itself. More importantly, the steel layer is made of a prototypic reactor vessel steel. The steel heater is arranged in such a way that the heat-removal surface is the original surface of the steel vessel after the vessel strippable protective paint layer was taken off. After the paint was stripped off, the steel was also subjected to a heat treatment at 500°C for a short period. This treatment, causing steel surface oxidation and aging, mimics thermal conditions the reactor vessel lower head is subjected to during normal reactor operation.

4.2. Experimental procedure

In boiling tests with de-inonized and tap waters, the experimental procedure is straight-forward. In tests where chemical solutions are used, the solutions are prepared in a separate volume. Chemical powders are dissolved in de-inonized (DI) water to reach a desired pH level, and then poured into the test section prior to heating. During boiling, de-inonized water is added to the test section to compensate for the vapor mass that escapes the test section without altering the concentration of chemicals in it. Post-test pH measurements show that the solution's pH remains at the initial level.

Heat-transfer surfaces were optically scanned prior to each experimental series. The surfaces are scanned after the experimental run for comparison. Significant surface changes were observed after boiling tests using chemicals, while no significant surface changes were observed after tests using de-inonized water.

In each experimental run, the power supply is regulated to provide an incremental power stepping. On each power level, the boiling process is allowed to run 3 to 5 minutes. This is to be compared to a thermal response time of the copper block estimated to be less than one minute. Most importantly, a thermocouple embedded in the copper block (0.5 mm from the copper block surface) is used to monitor whether a steady state was achieved before switching the power to a next level.

Figure 4.2 shows power and temperature history for a DI water run on a fresh copper heater surface, test U0331C. It can be seen that the thermocouple shows a nearly constant temperature over the whole 40-minute period of pool boiling till burnout. For steel heaters, the steel layer above the copper block presents significant thermal resistance, contributing to a temperature increase with each heat flux stepping and requiring a longer period to reach a steady state (Figure 4.3).

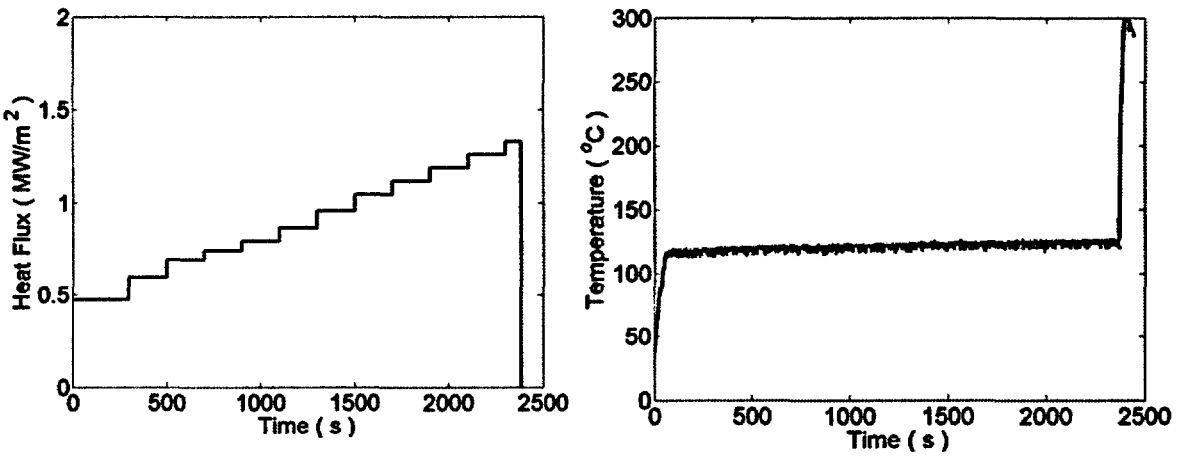

Figure 4.2. Power and temperature histories in run, C1-E (copper).

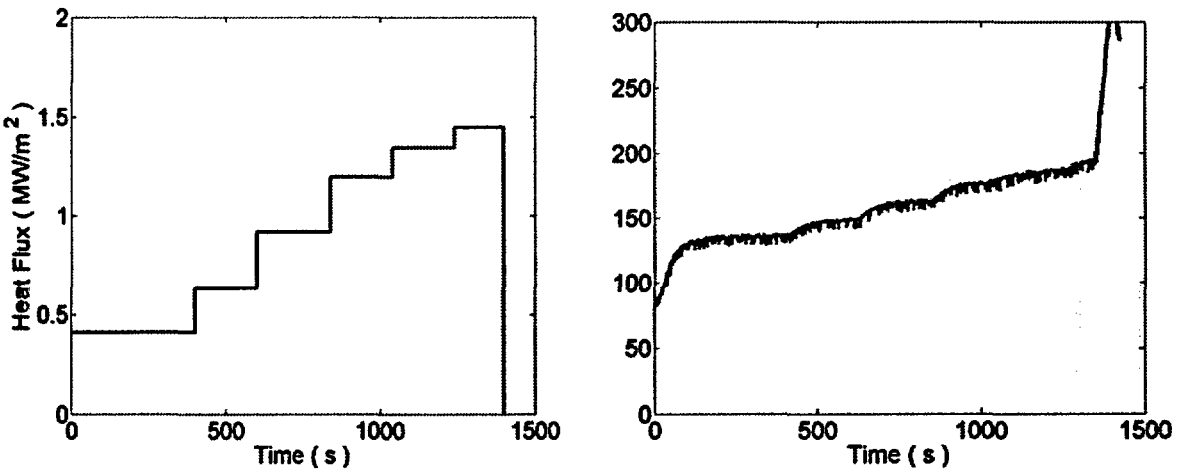

Figure 4.3. Power and temperature histories in run, S1-D (steel).

4.3. Experimental results

A total of 27 CHF determinations in 8 series of runs were made, as summarized in Table 4.1. Each series starts with a fresh (clean) sand-blasted surface. Within each series the surface condition is as delivered from the previous run, after cooldown, and rinsing of the whole test section with DI water. In the following we delineated the main trends contained in Table 4.1.

(a) Effect of surface material and aging by exposure to air and to boiling. This pertains to all runs made with pure DI water. In tests C1-A to C1-E, we can see that with increasing aging the CHF increases from a low value of ~ 750 kW/m^2 to over ~ 1,300 kW/m^2. In test C3-B we see that surface "pre-treatment" by boiling BA water to burnout yields a still further increase to over ~ 1,500 kW/m^2. Finally in tests S1-A and S1-B we see that fresh steel is as good as well aged copper (C1-E), and that further aging of steel produces rather modest improvement in CHF. All these results are very consistent with our recent basics-oriented BETA tests with nanofilm heaters and infrared thermography (Theofanous et al 2002).

(b) Effect of alkaline TSP water and acidic BA water. The TSP produced the highest CHF values yet, at ~ 1,800 to 1,900 kW/m^2, and this is consistent in both copper and steel surfaces as seen in runs C5-A, C6-A, S1-E, S1-F, S1-L, and S1-M. This is an important new result of basic as well practical significance. In BA water on the other hand the CHF exceeds that seen with DI water on aged heaters, reaching up to ~1500 kW/m^2, again consistently with both copper and steel surfaces, fresh as well as aged (C4-A, S1-I, S1-J, S1-K). Diluting the TSP water seems to diminish the performance in steel (S1-G) but not in copper (C6-A), but the data in this area are too few for definitive conclusion.

(c) As secondary effect we note that boiling tap water in effect produces instant aging of copper surfaces (C2-A, C2-B), while it has no effect on the already aged steel surfaces (S1-C, S1-D). Also, from one run (C7-A) there is a hint that BA may interfere with the beneficial effect of TSP, somewhat.

The overarching conclusion of these results is that TSP is very beneficial to CHF performance, while other chemicals found in tap water, and BA act mainly to age a copper surface to levels similar to those found naturally on a clean vessel steel surface. Also there is indication that these chemicals, acting principally through deposition processes, may interfere with the beneficial effect of TSP.

Table 4.1. Critical Heat Flux experiments on copper (BETA-C) and steel (BETA-S) heaters, with different waters. Heavy lines separate different test series, each beginning with fresh, sand-blasted surface.

Run ID	Heater	Coolant	Heater surface condition. Test procedure and specifics	CHF kW/m^2
C1-A	Copper	DI Water	Fresh sand blasted surface. Run one hour.	758
C1-B	Copper	DI Water	Air exposure 24 hours. Run 25 minutes.	743
C1-C	Copper	DI Water	Air exposure 72 hours. Run 25 minutes.	933
C1-D	Copper	DI Water	Air exposure 1 hour. Run 30 minutes.	1110
C1-E	Copper	DI Water	Air exposure 4 hours. Run 40 minutes.	1259
C1-F	Copper	Tap Water	Air exposure 16 hours. Run 40 minutes.	1321
C2-A	Copper	Tap Water	Fresh sand blasting surface. Run 30 min.	1121
C2-B	Copper	Tap Water	Air exposure 5 hours. Run 35 minutes.	1400[a]
C3-A	Copper	BA in DI	Fresh sand blasted surface. pH@4.5	1463
C3-B	Copper	DI water		1549
C4-A	Copper	BA in DI	Fresh sand blasted surface. pH@4.5	1500[b]
C5-A	Copper	TSP in DI	Fresh sand blasted surface. pH@14	1710
C6-A	Copper	TSP in DI	Fresh sand blasted surface. pH@8	1805
C7-A	Copper	BA-TSP in DI	Fresh sand blasted surface. BA pH@4.5, then add TSP pH@8	1600[c]
S1-A	Steel	DI Water	Original vessel steel surface	1322
S1-B	Steel	DI Water	Reproducibility check	1368
S1-C	Steel	Tap Water	pH@7	1361
S1-D	Steel	Tap Water	pH@7	1346
S1-E	Steel	TSP in DI	pH@14	1800[d]
S1-F	Steel	TSP in DI	pH@14	1816
S1-G	Steel	TSP in DI	pH@11	1595
S1-H	Steel	DI	Examine lingering effect of TSP	1575
S1-I	Steel	BA in DI	pH@4.5	1567[e]
S1-J	Steel	BA in DI	pH@4	1373
S1-K	Steel	BA in DI	pH@4	1500[g]
S1-L	Steel	TSP in DI	pH@13	1847[h]
S1-M	Steel	TSP in DI	pH@14	1872

In Table 4.1:

- ✓BA – Boric Acid; TSP – TriSodium Phosphate, DI – De-Inonized water;
- ✓CHF determined by input power one step before the step where burnout detected, except (a-h);
- ✓(a), (c) (d): CHF is approximated between two power levels.
- ✓(b): CHF is defined at the power step where significant temperature fluctuations are observed;
- ✓(e), (h): CHF are taken at the burnout due to long time duration prior to temperature escalation.

5. SYNTHESIS OF ULPU-V AND BETA TEST RESULTS

As noted in the previous section the BETA tests provide a principal connection between the aged copper heaters in ULPU and the prototypic steel material relevant to the AP1000 IVR. While established under pool boiling conditions, this connection is very tight in general, as both sets of data indicate the dominant influence of surface material aging, under both pool and flow boiling conditions, and convergence of CHF trends with degree of aging.

Moreover, the data elucidate the role of dissolved substances, and impurities, in the coolant to modify the behavior in a way similar to the natural aging obtained by heating in air or boiling in pure water. All the details in this respect are not completely understood (at the basic level) yet, but both ULPU and BETA results provide an abundance of evidence that this aging effect is strong and rapid, yielding a significantly enhanced CHF performance relative to that found under singularly pure conditions.

On this basis with the currently optimal baffle position found in test series M63, the appropriately critical heat flux value for AP1000 IVR evaluation at the relevant upper positions of $66^{\circ} < \theta < 90^{\circ}$, is in the 1,800 to 2,000 kW/m^2 range. These values do not contain the enhancing effect of TSP found in BETA, and may, therefore, be conservative.

6. CONCLUSIONS AND RECOMMENDATIONS

- A streamlined geometry such as employed in ULPU Configurations IV and V was shown to significantly increase the previously defined coolability margins in connection with the AP600 certification. Moreover, the deeper, more specific to AP1000 study in Configuration V revealed additional coolability margins relative to Configuration IV results.

- Under representative AP1000 exit geometry (at the RPV nozzle gallery), the natural circulation flow is dominantly subcooled, and is modulated by periodic flashing, and frictional phenomena at the exit. We recommend a closer examination of the effect of exit flow resistance on these phenomena, the natural circulation flow rate, and on the CHF performance.

- Heated surface chemistry and nanomorphology, and coolant chemistry and impurities can have a profound influence on cooling performance, further enhancing this understanding from previous ULPU tests. We use the term "aging" to describe the aggregate of these not-yet-fully-understood, molecular scale phenomena. An aged copper surface such as that employed in ULPU exhibits a similar coolability performance as the bare external surface of the RPV steel. We recommend that peelable protective coating be used in shipment, and that it be removed on installation.

- At normal aging conditions as generally relevant in technical large scale systems, and waters containing microscopic impurities and dissolved substances, the AP1000-related coolability limits at the upper region ($66^\circ < \theta < 90^\circ$) of the lower head is in the 1.8 to 2.0 MW/m^2 range. The normally found in containment waters TSP can deliver outstanding further enhancement in performance, but the effect can be interfered by the presence of other substances and this remains unquantified at this time. We recommend a closer examination of this, in conjunction with reducing the exit flow resistance in ULPU as recommended above.

- The main energy content of the dynamic loads generated is due to cyclic boiling-condensing phenomena in the vicinity of the lower head, and flashing-sweeping phenomena at the upper end. Amplitudes and spectra provided in this report can be used in the structural design of the thermal insulation that is to form the flow path.

7. REFERENCES

T.G., Theofanous, C. Liu, S. Additon, S. Angelini, O. Kymäläinen, and T. Salmassi, In-Vessel Coolability and Retention of a Core Melt, DOE/ID-10460, October 1996.

T.G. Theofanous, and S. Syri, The Coolability Limits of a Reactor Pressure Vessel Lower Head, Nuclear Engineering and Design **169** (1997) 59-76.

T.G. Theofanous, J.P. Tu, T. Salmassi and T.N. Dinh, 2002a "Quantification of Limit to Coolability in ULPU-2000 Configuration IV", CRSS Technical Report 02/05-1, May-December 2002.

T.G. Theofanous, J.P. Tu, A.T. Dinh and T.N. Dinh, 2002b, "The Boiling Crisis Phenomenon – Part 1: Nucleation and Nucleate Boiling Heat Transfer", *J. Experimental Thermal and Fluid Science*, pp.775-792, V.26 (6-7) Aug 2002.

T.G. Theofanous, T.N. Dinh, J.P. Tu, and A.T. Dinh, 2002c, "The Boiling Crisis Phenomenon – Part 2: Dryout Dynamics and Burnout", *J. Experimental Thermal and Fluid Science*, V.26 (6-7), pp.793-810.

DISCLAIMER

This report was prepared as an account of a research project conducted at the University of California Santa Barbara Center for Risk Studies and Safety and sponsored by U.S. Department of Energy's International Nuclear Energy Research Initiative program. Neither the United States Government not any agency thereof, nor any of their employees, nor the University of California and its employees, makes any warranty, express or implied, or assumes any legal liability or responsibility for the agency and the University, completeness, or usefulness of any information, apparatus, product or process disclosed, or represents that its use would not infringe privately owned right. The views and opinions of authors expressed therein do not necessarily state or reflect those of the United States Government or any agency thereof or the University of California.